Histone H2B Monoubiquitylation Regulates Elongation-to-Termination Transition in RNA Polymerase II Transcription

Tirthankar Bandyopadhyay[1], Baidehi Basu[1], Pabitra K. Parua[1*]

[1]Department of Molecular Pharmacology, Albert Einstein College of Medicine, Bronx, NY 10461

***Corresponding author:**

Pabitra K. Parua, Department of Molecular Pharmacology, Albert Einstein College of Medicine, 1300 Morris Park Avenue, Bronx, NY 10461, USA. Phone: (718) 430-4284. Email: pabitra.parua@einsteinmed.edu

RNA Polymerase II (Pol II)-dependent transcription is meticulously regulated during initiation, elongation, termination, and two pivotal transitions: from initiation to elongation and from elongation to termination [1]. The successful transition from

elongation to termination is vital for accurate transcription termination [2,3]. While elongation and termination have been extensively studied, the regulatory mechanisms governing the transition between these stages are not fully understood. Here we report that, in fission yeast *Schizosaccharomyces pombe* (*S. pombe*) and human cells, Cdk9 and its cyclin partner (Cyclin T in humans, and Pch1 in *S. pombe*) disengage from the elongation machinery near gene 3'-ends, as Pol II crosses the cleavage and polyadenylation signal (CPS). Concurrently, chromatin immunoprecipitation (ChIP) data shows an increased association of Dis2 (the PP1 ortholog in *S. pombe*)[4] beyond the CPS. Additionally, ChIP-seq indicates that histone H2B monoubiquitylation (H2Bub1) is pivotal for Cdk9 occupancy but serves differential roles along the gene. H2Bub1 facilitates Cdk9 chromatin recruitment during elongation but prompts Cdk9 dissociation from the elongation complex as Pol II traverses the CPS. Furthermore, in *S. pombe*, disruptions of H2Bub1 in *htb1-K119R* [5] and sustained levels in *ubp8D* [6] inversely affect the chromatin occupancy of Pol II, Pol II CTD phosphorylation within the heptad repeats, Spt5, phosphorylated Spt5 (pSpt5), Dis2, components of the mRNA 3'-end processing complex (Pfs2 and Pla1), and termination factors Rhn1 (Rtt103) and Pcf1 around the CPS—diminishing with H2Bub1 loss and increasing with H2Bub1 stabilization. In essence, our data indicates that the H2Bub1-mediated eviction of Cdk9 as Pol II navigates the CPS precipitates a rise in PP1 binding, which, in turn, dephosphorylates pSpt5, slowing Pol II to facilitate efficient termination. The unique modulation of Cdk9 occupancy by H2Bub1 during transcription progression presents a compelling, novel concept requiring further exploration.

The elongation to termination transition in RNA Polymerase II (Pol II)-dependent transcription is regulated by a switch mechanism involving cyclin-dependent kinase 9 (Cdk9) and protein phosphatase 1 (PP1) that modulates the phosphorylation of Spt5 (Fig. 1a) [7]. Yet, the

53 precise mechanisms overseeing the activity switch of Cdk9 and PP1, as Pol II transits through
54 the cleavage and polyadenylation sequence (CPS), remain undefined. While investigating the
55 mechanism of timely reversal of Cdk9-PP1 activity (Fig. 1a) we hypothesized that either Cdk9
56 becomes inactive or dissociates from the elongation complex as Pol II transits through the CPS.
57 To understand the distribution of Cdk9 and its cyclin partner cyclin T1 (CycT1; Pch1, ortholog of
58 CycT1 in fission yeast) we conducted ChIP experiments in *Schizosaccharomyces pombe* (*S.*
59 *pombe*). The ChIP-qPCR results showed a gradual decrease of the chromatin occupancy of
60 Cdk9 and Pch1 towards the 3'-end of *psu1*$^{+}$, *pgk1*$^{+}$, and *pyk1*$^{+}$—more predominant
61 corresponding to the amplicon positioned beyond the CPS of these genes (Extended Data Fig.
62 1a-c). The ChIP-seq browser tracks indicate a diminished level of Cdk9 and Pch1 beyond the
63 CPS of *exg1*$^{+,}$ *eno101*$^{+}$, *pma1*$^{+}$ and *act1*$^{+}$ (Fig. 1b, Extended Data Fig. 1d). Wherever the
64 chromatin occupancy of Cdk9 and Pch1 dropped, Pol II and Spt5 accumulated, but pSpt5
65 reduced (Fig. 1b). The metagene plots further supported the notion of a global decrease in the
66 chromatin occupancy of Cdk9 and Pch1 as Pol II approaches the 3'-end of genes, with a
67 pronounced reduction beyond the CPS (Fig. 1c,d; Extended Data Fig. 1e,f). Similar to protein-
68 coding genes, the occupancy of Cdk9 and Pch1 decreases at the 3'-end of small nucleolar RNA
69 (snoRNA) coding genes (Extended Data Fig. 1g).

70 Similar to *S. pombe*, in human cells, the ChIP-qPCR distributions of Cdk9 across *cMYC,*
71 *ERRFI1*, *GAPDH* and *VEGFA* showed the gradual reduction of Cdk9 occupancy towards the 3'-
72 end of those genes (Extended Data Fig. 2a-d). The ChIP-seq browser tracks of four
73 representative genes (*TGIF1*, *KITLG*, *AREG*, and *ERRFI1*) indicated diminished levels of Cdk9
74 beyond the CPS, where Pol II and Spt5 peaked but the Spt5 CTR1 (C-terminal repeat region 1)
75 phosphorylation (Spt5-pCTR1) dropped (Fig. 1e, Extended Data Fig. 2e). Furthermore,
76 metagene plots demonstrated a global decrease in Cdk9 chromatin occupancy beyond the CPS
77 at location corresponding to the 3'-paused Pol II (Fig. 1f, Extended Data Fig. 2f-h). Overall,

78 these findings suggested that Cdk9 dissociated from the elongation complex as Pol II traverses
79 the CPS and this phenomenon is conserved in *S. pombe* and human.

80 Previous studies have shown that during elongation, Cdk9-mediated phosphorylation
81 inhibits the activity of Dis2, a PP1 ortholog in *S. pombe*, and reduces its chromatin occupancy [7].
82 In this study, we demonstrate the dissociation of Cdk9 from the elongation complex as Pol II
83 traverses the CPS. Drawing from consistent findings in both *S. pombe* and human studies, we
84 propose that the disengagement of Cdk9 and its partner CycT (Pch1) from the elongation
85 complex leads to increased chromatin occupancy of Dis2. The ChIP-qPCR analysis in *S. pombe*
86 indicates a dramatic incline in the occupancy of Dis2 beyond the CPS of the representative
87 genes, *psu1*$^{+}$, *pgk1*$^{+}$ and *pyk1*$^{+}$ (Fig. 2a-c, Extended Data Fig. 3a-c). The ChIP-seq browser
88 tracks for the sample genes display a significant buildup of Dis2 past the CPS, aligning with the
89 location of the 3'-paused Pol II (Fig. 2d, Extended Data Fig. 3d). Metagene analyses further
90 indicated a gradual increase in Dis2 occupancy towards the 3'-end of Pol II-transcribed genes,
91 with a sharp peak beyond the CPS (Fig. 2e, Extended Data Fig. 3e). To the best of our
92 knowledge, this is the first report detailing the genome-wide distribution of Dis2 (PP1),
93 demonstrating significant accumulation of Dis2 beyond the CPS. Overall, our results suggested
94 an inverse relationship between Cdk9 and Dis2: as the former leaves the elongation complex,
95 the latter begins to accumulate. This accumulation likely explains the Dis2-mediated rapid
96 dephosphorylation of pSpt5 beyond the CPS [7], which in turn appears to slow Pol II, promoting
97 faithful termination. However, the question remains: What triggers the eviction of Cdk9 from the
98 elongation complex during the transition from elongation to termination?

99 Earlier studies identified the functional interconnection between Cdk9 and the mono-
100 ubiquitylation of histone H2B (H2Bub1) at K120 in humans (K123 in *S. cerevisiae*, and K119 in
101 *S. pombe*) [8]. A decrease in Cdk9 activity negatively impacts the stability of H2Bub1, partly
102 through the phosphorylation of Spt5, which facilitates the formation of H2Bub1 [9-14]. In a
103 feedback scenario, H2Bub1, which is highly enriched in the gene bodies of active genes and

104 sharply decreases after the CPS [15,16], also controls Cdk9 recruitment in *S. pombe* [8] and human
105 cells [17,18]. The loss of H2Bub1 levels decreases chromatin occupancy of Cdk9 on gene body,
106 although this has been explored only at a limited number of loci. We propose that H2Bub1
107 preserves the chromatin occupancy of Cdk9 during the elongation phase of transcription, and
108 the loss of H2Bub1 as Pol II traverses the CPS might trigger the disengagement of Cdk9 from
109 the elongating Pol II complex. The ChIP-seq browser tracks showed that across the genes
110 *act1*$^+$, *exg1*$^+$, and *eno101*$^+$, disruption of H2Bub1 led to a decrease in Cdk9 occupancy at the 5'-
111 end and within the gene body (Fig. 3a, Extended Data Fig. 4a). However, upstream and
112 downstream of the CPS, the Cdk9 occupancy was increased in *htb1-K119R* cells compared to
113 wildtype. The metagene plot showed a sharp increase in Cdk9 occupancy around the CPS upon
114 loss of H2Bub1 (Fig. 3b, Extended Data Fig. 4b). The upstream increase of Cdk9 occupancy
115 indicates H2Bub1 rearranges Cdk9 association with the elongation complex before Pol II
116 passes through the CPS. These results suggest that H2Bub1 differentially impacts the
117 chromatin occupancy of Cdk9 across a transcription cycle. The decrease in Cdk9 occupancy
118 upon loss of H2Bub1 at the 5'-end to gene body is consistent with the previous findings
119 determined by ChIP-qPCR for a few genes [8]. However, the effects of H2Bub1 on Cdk9
120 occupancy at the 3'-end of genes have not been examined before. These potential paradigm-
121 shifting roles of H2Bub1 in regulating Cdk9's occupancy differentially across a gene is intriguing
122 and warrant further investigation.
123 Should H2Bub1 regulate Cdk9 occupancy during the elongation to termination transition,
124 we anticipated observing reversal of H2BK119R-phenotype in distribution of Cdk9 when H2B
125 undergoes hyper-monoubiquitylation. To examine this, we checked Cdk9 distribution in *ubp8D*
126 cells by ChIP-seq. Ubp8 serves as a ubiquitin C-terminal hydrolase in the SAGA complex and
127 its absence fortifies H2Bub1 at K119. In *ubp8D* cells, the ChIP-seq browser tracks showed a
128 reduced level of Cdk9 towards the 3'-end of the genes *act1*$^+$, *exg1*$^+$, and *eno101*$^+$ (Fig. 3c,
129 Extended Data Fig. 4a). The metagene plot revealed no accumulation of Cdk9 upstream of the

130 CPS; however, a sharp and widespread decline in Cdk9 occupancy beyond the CPS upon Ubp8
131 loss (Fig. 3d, Extended Data Fig. 4c). These observations reinforced our hypothesis that hyper-
132 monoubiquitylation of H2B, situated upstream of the CPS [16], aids in dislodging Cdk9 from the
133 elongation complex as it traverses the CPS. Accordingly, the loss of H2Bub1 engages Cdk9
134 around the CPS.

135 We identified an inverse relationship between Cdk9 and Dis2 distribution throughout the
136 transcription cycle. We expanded our studies to determine whether H2Bub1 inversely regulates
137 Dis2 occupancy relative to Cdk9. To investigate this, we examined Dis2 occupancy in *htb1-*
138 *K119R* and *ubp8Δ* cells using ChIP. The ChIP-qPCR results indicate that the loss of H2Bub1
139 decreases Dis2 occupancy, specifically beyond the CPS of three genes, *psu1+*, *pgk1*$^{+}$ and *pyk1*$^{+}$
140 (Fig. 3e; Extended Data Fig. 4d,e, top panel). Conversely, persistent levels of H2Bub1 increase
141 Dis2 occupancy in the same region (Fig. 3f; Extended Data Fig. 4d,e, bottom panel). In *htb1-*
142 *K119R* cells, consistent with the alterations in Cdk9 and Dis2 occupancy, ChIP-seq browser
143 tracks show an increase in Spt5 phosphorylation (pSpt5) around the CPS and a decrease at the
144 5'-end of genes, respectively (Fig. 3g, Extended Data Fig. 5a,b). However, in agreement with
145 previous reports, Spt5 phosphorylation decreases in whole-cell extracts following the loss of
146 H2Bub1 (in *htb1-K119R* cells), whereas it increases upon stabilization of H2Bub1 in *ubp8Δ* cells
147 [8] (Extended Data Fig. 5c). Presumably, the loss of Spt5 phosphorylation from the 5'-end to the
148 middle of the gene body seen in *htb1-K119R* cells accounts for the global decrease in whole-cell
149 extracts. Metagene analyses reveal a sharp accumulation of pSpt5 levels around the CPS in
150 *htb1-K119R* cells (Fig. 3h, Extended Data Fig. 5d). However, in *ubp8Δ* cells, pSpt5 decreases
151 around the CPS (Fig. 3i, Extended Data Fig. 5e,f), agreeing with the accumulation of H2Bub1
152 upstream of the CPS, where pSpt5 decays progressively [16]. Overall, our results demonstrate
153 that H2Bub1 inversely regulates Cdk9 and Dis2 occupancy during the transition from elongation
154 to termination, leading to the modulation of Spt5 phosphorylation.

155 The transition from elongation to termination is closely linked with pre-mRNA 3'-end
156 cleavage and polyadenylation. Once Pol II transcribes the cleavage and polyadenylation
157 sequence, the cleavage and polyadenylation factor (CPF), a multiprotein complex, is recruited.
158 This in turn facilitates the 3'-end cleavage and polyadenylation of pre-mRNA [19]. We sought to
159 determine whether the cleavage and polyadenylation of pre-mRNA triggers the dissociation of
160 Cdk9 from the elongation complex. To investigate this, we conducted Cdk9 ChIP in *pfs2-11*
161 cells. Since Pfs2 is a crucial component of the CPF complex, the *pfs2-11* mutant shows a
162 deficiency in mRNA 3'-end processing at 37°C [20]. ChIP-qPCR analysis demonstrated that there
163 were no changes in Cdk9 distribution on representative genes following the heat inactivation of
164 Pfs2 (Extended Data Fig. 6a,b). This finding aligns with previous reports showing no changes in
165 CPF occupancy when Cdk9 is inhibited and no alterations in chromatin-bound levels of Spt5
166 phosphorylation upon Pfs2 heat inactivation [7]. However, under these same conditions, Pol II
167 occupancy increased at the 3'-end of the genes, suggesting termination defects. These findings
168 suggest that: 1) the productive cleavage and polyadenylation event is not the trigger for Cdk9's
169 dissociation from the elongation complex; it is either independent of or occurs prior to mRNA
170 cleavage and polyadenylation, and 2) the accumulation of Cdk9 upon loss of H2Bub1 is not due
171 to the accumulation of Pol II.
172 These results invoked us to determine whether H2Bub1 regulates the recruitment of
173 CPF complex. To investigate that we conducted ChIP-qPCR for Pla1, mRNA cleavage and
174 polyadenylation specificity factor poly(A) polymerase, and Pfs2 in *htb1-K119R* and *ubp8Δ* cells.
175 The ChIP-qPCR results show a decrease or an increase or in both Pfs2 (Extended Data Fig.
176 6c,d) and Pla1 (Extended Data Fig. 6e,f) recruitment beyond the CPS of the representative
177 genes when H2Bub1 is disrupted (in *htb1-K119R* cells) or persistent (in *ubp8Δ* cells),
178 respectively. These results indicate that H2Bub1 facilitates the recruitment of CPF complex.
179 Moreover, these effects of H2Bub1 on the occupancy of these two factors of the 3'-end
180 processing complex, are opposite of the effects on the occupancy of Cdk9 at the similar regions.

181 Additionally, our results imply that H2Bub1-mediated Cdk9 eviction happens upstream of 3'-end
182 processing.

183 Previous studies report that PP1-mediated Spt5 dephosphorylation facilitates Pol II
184 slowing beyond the CPS [7]. This slow Pol II favors faithful termination by allowing the recruitment
185 of termination factors. In our current study, we found that the loss of H2Bub1: 1) leads to
186 accumulation of Cdk9 around the CPS, 2) disrupts the chromatin occupancy of Dis2,
187 subsequently, 2) increases the Spt5 phosphorylation beyond the CPS, and 3) decreases the
188 association of cleavage and polyadenylation factors with the elongation complex, which is
189 required for proper 3'-end processing of mRNA. Given that Spt5 dephosphorylation and proper
190 3'-end processing are essential for faithful termination, we aimed to investigate whether H2Bub1
191 regulates termination. To examine this, we conducted Pol II ChIP-seq in *htb1-K119R* and *ubp8Δ*
192 cells. In *htb1-K119R* cells, the ChIP-seq bowser tracks showed a wider distribution of Pol II past
193 the CPS, indicating readthrough transcription (Fig. 4a,b, Extended Data Fig 7). Conversely, in
194 cells lacking Ubp8 (*ubp8Δ*), there was a tighter distribution of Pol II around the termination
195 region, which suggests a more effective termination process (Fig. 4a,b, Extended Data Fig 7).
196 Interestingly, Cdk9 inhibition in *htb1-K119R* cells narrowed the Pol II distribution beyond the
197 CPS, indicating a rescue of the termination defects observed in these cells (Fig. 4a,b, Extended
198 Data Fig 7). This result suggests that the accumulation of Cdk9 following the loss of H2Bub1 is
199 the primary trigger for the termination defects by disrupting Dis2 recruitment and subsequently
200 stabilizing Spt5 phosphorylation. To investigate the termination defects further, we performed
201 regular PCR and RT-qPCR for selected regions upstream and downstream of the CPS. The
202 DNA gel and RT-qPCR showed transcript production beyond the canonical termination zone of
203 *psu1*$^{+}$, *pgk1*$^{+}$, *pyk1*$^{+}$ and *pho1*+ genes in *htb1-K119R* cells, implying readthrough transcription
204 (Fig. c, Extended Data Fig 8).

205 In investigating the molecular mechanisms of termination defects upon disruption of
206 H2Bub1, we conducted ChIP for the termination factors, Pcf11, and Rhn1 (Rtt103). ChIP-qPCR

207 showed a significant reduction in the occupancy of the termination factors Rhn1 and Pcf11 past
208 the CPS in *htb1-K119R* cells (Fig. 4d, Extended Data Fig. 9a,c). However, in Ubp8-deficient
209 backgrounds, there was a marked increase in the chromatic occupancy of Rhn1 and Pcf11
210 beyond the CPS (Fig. 4e, Extended Data Fig. 9b,d). Thus, the impairment in the recruitment of
211 termination factors can explain the termination defects *in htb1-K119R* cells. During termination,
212 the phosphorylation of Tyr1 (pTyr1) and Ser2 (pSer2) within Pol II CTD heptad repeats assists in
213 recruiting mRNA 3'-end processing and termination factors [21-24]. The ChIP-qPCR results indicate
214 a substantial decrease in both pTyr1 and pSer2 levels following the disruption of H2Bub1 in
215 *htb1-K119R* cells (Fig. 4f, Extended Data Fig 10a,b,e,f), with only minimal or no changes
216 observed in *ubp8Δ* cells (Fig. 4g, Extended Data Fig. 10c,d,g,h). Consistently, immunoblot
217 revealed a significant decrease in pTyr1 and pSer2 levels in whole cell extract upon the loss of
218 H2Bub1; however, these marks remained unchanged following the stabilization of H2Bub1
219 (Extended Data Fig. 10i). Consequently, the changes observed in the chromatin occupancy of
220 Rhn1 and Pcf11 in both *htb1-K119R* and *ubp8Δ* strains seem to result directly from the altered
221 levels of pTyr1 and pSer2 on chromatin. In conclusion, our findings suggest that hyper-
222 monoubiquitylation ensures faithful termination by: (i) facilitating the dissociation of Cdk9 from
223 the elongation complex as Pol II traverses the CPS, thus (ii) increasing Dis2's occupancy and
224 the subsequent dephosphorylation of Spt5, (iii) enhancing the recruitment of cleavage and
225 polyadenylation factors for proper 3'-end processing of mRNA, (iv) subsequently increasing the
226 phosphorylation levels of Tyr1 and Ser2 on the Pol II CTD, which in turn facilitates (v) the
227 chromatin recruitment of termination factors (Fig. 4h; top panel). Actually, in physiological
228 conditions, H2Bub1 accumulates just upstream of the CPS, where pSpt5 gradually decays,
229 explaining its decisive role in the elongation-to-termination transition (Extended Data Fig. 10j) [16].
230 However, the loss of H2Bub1 leads to the accumulation of Cdk9 around the CPS, reversing all
231 downstream sequential events and resulting in termination defects (Fig. 4h; bottom panel). Our
232 findings highlight the need for further investigation to uncover the molecular mechanisms by

which H2Bub1 differentially regulates Cdk9's chromatin occupancy throughout the transcription cycle.

The major roles of H2Bub1 in transcription regulation have been depicted in the stages of initiation and elongation. However, the direct role of H2Bub1 in regulating the transition from elongation to termination has not been reported earlier. Therefore, identifying the role of H2Bub1 in termination is novel and adds a new layer of mechanism in transcription regulation. It would be interesting in the future to investigate how H2Bub1 regulates Cdk9 occupancy, pTyr1, and pSer2 during the elongation to termination transition. Does H2Bub1 influence the recruitment of the kinase(s) and/or phosphatase(s) of pTyr1 and pSer2? Several mechanistic explanations for the role of H2Bub1 in transcription have already been proposed. H2Bub1 stimulates FACT-mediated displacement of an H2A/H2B dimer from the core nucleosome, thereby enhancing the passage of Pol II through the nucleosome [25]. H2Bub1 promotes the reassembly of nucleosomes in the wake of elongating Pol II [26,27]. Moreover, H2Bub1 regulates transcription by facilitating the recruitment of Set1, a component of the COMPASS complex (MLL complex in humans), and by Dot1, which catalyzes the methylation of histone H3 lysine 4 (H3K4me) and 79 (H3K79me), respectively [28-30]. These two marks are linked to active transcription. Therefore, in the future, it would be interesting to determine whether any of these mechanisms play intermediate roles in regulating the chromatin occupancy of Cdk9 by H2Bub1.

1 Parua, P. K. & Fisher, R. P. Dissecting the Pol II transcription cycle and derailing cancer with CDK inhibitors. *Nat Chem Biol* **16**, 716-724, doi:10.1038/s41589-020-0563-4 (2020).

2 Proudfoot, N. J. Transcriptional termination in mammals: Stopping the RNA polymerase II juggernaut. *Science* **352**, aad9926, doi:10.1126/science.aad9926 (2016).

3 Rodriguez-Molina, J. B., West, S. & Passmore, L. A. Knowing when to stop: Transcription termination on protein-coding genes by eukaryotic RNAPII. *Mol Cell* **83**, 404-415, doi:10.1016/j.molcel.2022.12.021 (2023).

4 Grallert, A. *et al.* A PP1-PP2A phosphatase relay controls mitotic progression. *Nature* **517**, 94-98, doi:10.1038/nature14019 (2015).

5 Zofall, M. & Grewal, S. I. HULC, a histone H2B ubiquitinating complex, modulates heterochromatin independent of histone methylation in fission yeast. *J Biol Chem* **282**, 14065-14072, doi:10.1074/jbc.M700292200 (2007).

6 Helmlinger, D. *et al.* The S. pombe SAGA complex controls the switch from proliferation to sexual differentiation through the opposing roles of its subunits Gcn5 and Spt8. *Genes Dev* **22**, 3184-3195, doi:10.1101/gad.1719908 (2008).
7 Parua, P. K. *et al.* A Cdk9-PP1 switch regulates the elongation-termination transition of RNA polymerase II. *Nature* **558**, 460-464, doi:10.1038/s41586-018-0214-z (2018).
8 Sanso, M. *et al.* A positive feedback loop links opposing functions of P-TEFb/Cdk9 and histone H2B ubiquitylation to regulate transcript elongation in fission yeast. *PLoS Genet* **8**, e1002822, doi:10.1371/journal.pgen.1002822 (2012).
9 Wood, A., Schneider, J., Dover, J., Johnston, M. & Shilatifard, A. The Bur1/Bur2 complex is required for histone H2B monoubiquitination by Rad6/Bre1 and histone methylation by COMPASS. *Mol Cell* **20**, 589-599, doi:10.1016/j.molcel.2005.09.010 (2005).
10 Laribee, R. N. *et al.* BUR kinase selectively regulates H3 K4 trimethylation and H2B ubiquitylation through recruitment of the PAF elongation complex. *Curr Biol* **15**, 1487-1493, doi:10.1016/j.cub.2005.07.028 (2005).
11 Zhou, K., Kuo, W. H., Fillingham, J. & Greenblatt, J. F. Control of transcriptional elongation and cotranscriptional histone modification by the yeast BUR kinase substrate Spt5. *Proc Natl Acad Sci U S A* **106**, 6956-6961, doi:10.1073/pnas.0806302106 (2009).
12 Liu, Y. *et al.* Phosphorylation of the transcription elongation factor Spt5 by yeast Bur1 kinase stimulates recruitment of the PAF complex. *Mol Cell Biol* **29**, 4852-4863, doi:10.1128/MCB.00609-09 (2009).
13 Qiu, H., Hu, C., Gaur, N. A. & Hinnebusch, A. G. Pol II CTD kinases Bur1 and Kin28 promote Spt5 CTR-independent recruitment of Paf1 complex. *EMBO J* **31**, 3494-3505, doi:10.1038/emboj.2012.188 (2012).
14 Mayekar, M. K., Gardner, R. G. & Arndt, K. M. The recruitment of the Saccharomyces cerevisiae Paf1 complex to active genes requires a domain of Rtf1 that directly interacts with the Spt4-Spt5 complex. *Mol Cell Biol* **33**, 3259-3273, doi:10.1128/MCB.00270-13 (2013).
15 Minsky, N. *et al.* Monoubiquitinated H2B is associated with the transcribed region of highly expressed genes in human cells. *Nat Cell Biol* **10**, 483-488, doi:10.1038/ncb1712 (2008).
16 Sanso, M. *et al.* Cdk9 and H2Bub1 signal to Clr6-CII/Rpd3S to suppress aberrant antisense transcription. *Nucleic Acids Res* **48**, 7154-7168, doi:10.1093/nar/gkaa474 (2020).
17 Bres, V., Gomes, N., Pickle, L. & Jones, K. A. A human splicing factor, SKIP, associates with P-TEFb and enhances transcription elongation by HIV-1 Tat. *Genes Dev* **19**, 1211-1226, doi:10.1101/gad.1291705 (2005).
18 Bres, V., Yoshida, T., Pickle, L. & Jones, K. A. SKIP interacts with c-Myc and Menin to promote HIV-1 Tat transactivation. *Mol Cell* **36**, 75-87, doi:10.1016/j.molcel.2009.08.015 (2009).
19 Boreikaite, V. & Passmore, L. A. 3'-End Processing of Eukaryotic mRNA: Machinery, Regulation, and Impact on Gene Expression. *Annu Rev Biochem* **92**, 199-225, doi:10.1146/annurev-biochem-052521-012445 (2023).
20 Wang, S. W., Asakawa, K., Win, T. Z., Toda, T. & Norbury, C. J. Inactivation of the pre-mRNA cleavage and polyadenylation factor Pfs2 in fission yeast causes lethal cell cycle defects. *Mol Cell Biol* **25**, 2288-2296, doi:10.1128/MCB.25.6.2288-2296.2005 (2005).
21 Descostes, N. *et al.* Tyrosine phosphorylation of RNA polymerase II CTD is associated with antisense promoter transcription and active enhancers in mammalian cells. *Elife* **3**, e02105, doi:10.7554/eLife.02105 (2014).
22 Larochelle, M. *et al.* Common mechanism of transcription termination at coding and noncoding RNA genes in fission yeast. *Nat Commun* **9**, 4364, doi:10.1038/s41467-018-06546-x (2018).

316 23 Ahn, S. H., Kim, M. & Buratowski, S. Phosphorylation of serine 2 within the RNA
317 polymerase II C-terminal domain couples transcription and 3' end processing. *Mol Cell*
318 **13**, 67-76 (2004).
319 24 Bartkowiak, B. *et al.* CDK12 is a transcription elongation-associated CTD kinase, the
320 metazoan ortholog of yeast Ctk1. *Genes Dev* **24**, 2303-2316, doi:10.1101/gad.1968210
321 (2010).
322 25 Pavri, R. *et al.* Histone H2B monoubiquitination functions cooperatively with FACT to
323 regulate elongation by RNA polymerase II. *Cell* **125**, 703-717,
324 doi:10.1016/j.cell.2006.04.029 (2006).
325 26 Fleming, A. B., Kao, C. F., Hillyer, C., Pikaart, M. & Osley, M. A. H2B ubiquitylation plays
326 a role in nucleosome dynamics during transcription elongation. *Mol Cell* **31**, 57-66,
327 doi:10.1016/j.molcel.2008.04.025 (2008).
328 27 Batta, K., Zhang, Z., Yen, K., Goffman, D. B. & Pugh, B. F. Genome-wide function of
329 H2B ubiquitylation in promoter and genic regions. *Genes Dev* **25**, 2254-2265,
330 doi:10.1101/gad.177238.111 (2011).
331 28 Ng, H. H., Xu, R. M., Zhang, Y. & Struhl, K. Ubiquitination of histone H2B by Rad6 is
332 required for efficient Dot1-mediated methylation of histone H3 lysine 79. *J Biol Chem*
333 **277**, 34655-34657, doi:10.1074/jbc.C200433200 (2002).
334 29 Briggs, S. D. *et al.* Gene silencing: trans-histone regulatory pathway in chromatin.
335 *Nature* **418**, 498, doi:10.1038/nature00970 (2002).
336 30 Sun, Z. W. & Allis, C. D. Ubiquitination of histone H2B regulates H3 methylation and
337 gene silencing in yeast. *Nature* **418**, 104-108, doi:10.1038/nature00883 (2002).
338 31 Forsburg, S. L. Growth and manipulation of S. pombe. *Curr Protoc Mol Biol* **Chapter 13**,
339 Unit 13 16, doi:10.1002/0471142727.mb1316s64 (2003).
340 32 Forsburg, S. L. S. pombe strain maintenance and media. *Curr Protoc Mol Biol* **Chapter**
341 **13**, Unit 13 15, doi:10.1002/0471142727.mb1315s64 (2003).
342 33 Sabatinos, S. A. & Forsburg, S. L. Molecular genetics of Schizosaccharomyces pombe.
343 *Methods Enzymol* **470**, 759-795, doi:10.1016/S0076-6879(10)70032-X (2010).
344 34 Forsburg, S. L. & Rhind, N. Basic methods for fission yeast. *Yeast* **23**, 173-183,
345 doi:10.1002/yea.1347 (2006).
346 35 Bahler, J. *et al.* Heterologous modules for efficient and versatile PCR-based gene
347 targeting in Schizosaccharomyces pombe. *Yeast* **14**, 943-951, doi:10.1002/(SICI)1097-
348 0061(199807)14:10<943::AID-YEA292>3.0.CO;2-Y (1998).
349 36 Forsburg, S. L. Introduction of DNA into S. pombe cells. *Curr Protoc Mol Biol* **Chapter**
350 **13**, Unit 13 17, doi:10.1002/0471142727.mb1317s64 (2003).
351 37 Larochelle, S. *et al.* Cyclin-dependent kinase control of the initiation-to-elongation switch
352 of RNA polymerase II. *Nat Struct Mol Biol* **19**, 1108-1115 (2012).
353 38 Langmead, B. & Salzberg, S. L. Fast gapped-read alignment with Bowtie 2. *Nat Methods*
354 **9**, 357-359, doi:10.1038/nmeth.1923 (2012).
355 39 Feng, J., Liu, T., Qin, B., Zhang, Y. & Liu, X. S. Identifying ChIP-seq enrichment using
356 MACS. *Nat Protoc* **7**, 1728-1740, doi:10.1038/nprot.2012.101 (2012).
357 40 Ramirez, F. *et al.* deepTools2: a next generation web server for deep-sequencing data
358 analysis. *Nucleic Acids Res* **44**, W160-165, doi:10.1093/nar/gkw257 (2016).
359 41 Viladevall, L. *et al.* TFIIH and P-TEFb coordinate transcription with capping enzyme
360 recruitment at specific genes in fission yeast. *Mol Cell* **33**, 738-751,
361 doi:10.1016/j.molcel.2009.01.029 (2009).
362 42 Parua, P. K., Kalan, S., Benjamin, B., Sanso, M. & Fisher, R. P. Distinct Cdk9-
363 phosphatase switches act at the beginning and end of elongation by RNA polymerase II.
364 *Nat Commun* **11**, 4338, doi:10.1038/s41467-020-18173-6 (2020).
365 43 Saiz, J. E. & Fisher, R. P. A CDK-activating kinase network is required in cell cycle
366 control and transcription in fission yeast. *Curr Biol* **12**, 1100-1105 (2002).

367 44 Pei, Y. *et al.* Cyclin-dependent kinase 9 (Cdk9) of fission yeast is activated by the CDK-
368 activating kinase Csk1, overlaps functionally with the TFIIH-associated kinase Mcs6, and
369 associates with the mRNA cap methyltransferase Pcm1 in vivo. *Mol Cell Biol* **26**, 777-
370 788, doi:10.1128/MCB.26.3.777-788.2006 (2006).
371 45 St Amour, C. V. *et al.* Separate domains of fission yeast Cdk9 (P-TEFb) are required for
372 capping enzyme recruitment and primed (Ser7-phosphorylated) Rpb1 carboxyl-terminal
373 domain substrate recognition. *Mol Cell Biol* **32**, 2372-2383, doi:10.1128/MCB.06657-11
374 (2012).
375 46 Vanoosthuyse, V. *et al.* CPF-associated phosphatase activity opposes condensin-
376 mediated chromosome condensation. *PLoS Genet* **10**, e1004415,
377 doi:10.1371/journal.pgen.1004415 (2014).
378

379 **Acknowledgements** We thank Robert P. Fisher, Jason. C. Tanny B. Schwer, S. Shuman, and
380 V. Vanoosthuyse for providing yeast strains and antibodies; Robert C. Coleman, Matthew J.
381 Gamble and Ian Willis for manuscript reading and providing critical comments. This work was
382 supported by start-up fund from Montefiore-Einstein Cancer Center (MECC), Albert Einstein
383 College of Medicine.
384

385 **Author Contributions** T.B. conducted immunoblot analysis and performed ChIP-qPCR
386 analysis. T.B. conducted ChIP-seq and data analysis to map genome-wide distribution of Cdk9,
387 Pch1, Spt5, pSpt5, Pol II, and Dis2. B.B. isolated RNA from yeast and conducted RT-qPCR
388 analysis. P.K.P and T.B. generated yeast strains. P.K.P. and T.B. prepared the manuscript.
389

390 **Author Information** Correspondence and requests for materials should be addressed to
391 pabitra.parua@einsteinmed.edu
392

393 **METHODS**

394 **Yeast strains and growth conditions.** Yeast strains used in the study are listed in Extended
395 Data Table 1. Strains were grown in YES (5% yeast extract, 30% dextrose, 250 mg/l each of
396 adenine, leucine, lysine, histidine and uracil) media at 30°C[31,32], unless otherwise indicated.
397 New strains were generated by mating or random spore analysis[33,34]. Strains with epitope tags

398 and deletions were generated by homologous recombination of DNA fragments either
399 synthesized by PCR or fragmented from a donor plasmid[35,36]. Correct marker integration was
400 confirmed by PCR.
401
402 **Cell lines and media.** Colon carcinoma-derived HCT116 cells were cultured in McCoy's 5A
403 medium with L-glutamine (Corning) supplemented with 10% Fetal Bovine Serum (FBS, Gibco)
404 and 1x Penicillin-Streptomycin (Corning).
405
406 **Immunoblotting.** Antibodies used in this study recognized Pol II (BioLegend, Clone: CTD4H8,
407 Catalog No: 904004), Pol II CTD phospho Ser2 (Abcam; Catalog No. Ab5095), Pol II CTD
408 phospho Tyr1 (Active Motif; Catalog No. 61383), H2B (Active Motif; Catalog No. 39237),
409 H2Bub1(Active Motif; Catalog No. 39623) and phospho Spt5 or total Spt5 (*S. pombe*) (Dr.
410 Larochelle (21st Century Biochemicals; Pr1357) [8]. For immunoblot analysis, proteins were
411 separated by SDS-PAGE and transferred to Protran™ 0.45 µm nitrocellulose membranes
412 (Cytiva Amersham™). The membranes were probed with primary antibodies at dilutions
413 recommended by the suppliers. Immunoblots were developed with Horseradish Peroxidase
414 (HRP) conjugated donkey anti-rabbit (GE Healthcare Life Sciences; Catalog No. NA934V),
415 sheep anti-mouse (GE Healthcare Life Sciences; Catalog No. NA9310V) and Alexa Fluor-
416 coupled goat anti-rabbit (A21076, Life Technologies). Proteins were detected by enhanced
417 chemiluminescence (Pierce ECL Western Blotting Substrate, Thermo Scientific; Catalog No.
418 32106).
419
420 **Chromatin immunoprecipitation in fission yeast.** Chromatin immunoprecipitation (ChIP) was
421 performed as previously described [7,16].. Briefly, *S. pombe* cell cultures were grown in YES to an
422 $O.D_{600}$ of 0.5 – 0.6 and crosslinked with 1% formaldehyde for 15 minutes at room temperature.
423 Crosslinking was terminated by adding 2.5 M glycine to a final concentration of 125 mM for 5

424 minutes. Cells were pelleted by centrifugation, washed with cold 1x TBS (10 mM Tris pH 7.5,
425 150 mM NaCl), frozen on dry ice, and stored at -80°C. Cell pellets from 50 ml cultures were
426 resuspended in ChIP lysis buffer I (50 mM HEPES pH 7.5, 140 mM NaCl, 1 mM EDTA, 1%
427 Triton X-100, 0.1% Na-deoxycholate, 1 mM PMSF, and protease and phosphatase inhibitor
428 cocktail) and lysed in a Mini-Beadbeater-16 (BioSpec Products; Catalog No. 607) in the
429 presence of glass beads (0.1 mm diameter) (BioSpec Products; Cat. No. 11079101) at 4°C for 1
430 minute (with 1 minute intervals on ice). Lysates were centrifuged at 16,100 x g for 20 minutes at
431 4°C. Pellets containing chromatin were resuspended in 1 ml ChIP lysis buffer II (50 mM HEPES
432 pH 7.5, 140 mM NaCl, 1 mM EDTA, 1% Triton X-100, 0.1% SDS, 0.1% Na-deoxycholate, 1 mM
433 PMSF, and protease and phosphatase inhibitor cocktail) and transferred to 15 ml polycarbonate
434 tubes. Lysates were sonicated for 30 minutes at 4°C (30 seconds ON, 30 seconds OFF, output
435 setting high) using a water bath sonicator (Diagenode Bioruptor® Plus; Cat. No. B01020001),
436 transferred to new 1.5 ml tubes, and centrifuged at 16,100 x g for 20 minutes at 4°C. 250 – 300
437 µg of chromatin extract was incubated with antibodies, FLAG (SIGMA; Catalog No. F3165-
438 1MG), Myc (Clone: 9E10; BioLegend; Catalog No. 626802), Pol II (8WG16) (Biolegend; Catalog
439 No. 664906), Pol II CTD phospho Ser2 (Abcam; Catalog No. Ab5095), Pol II CTD phospho Tyr1
440 (Active Motif; Catalog No. 61383), V5 (PK) (Fortis Life Sciences; Catalog No. A190-120A), H2B
441 (Active Motif; Catalog No. 39237), H2Bub1(Active Motif; Catalog No. 39623), H3 (Active Motif;
442 Catalog No. 39763), phospho Spt5 [8] (*S. pombe*) (Dr. Larochelle (21st Century Biochemicals;
443 Pr1357), overnight at 4°C with constant nutation. Extracts from *S. cerevisiae* strain BY4742 were
444 also prepared in parallel and spiked into each immunoprecipitation (1% of the weight) for
445 normalization. The suspension was incubated at room temperature for an additional 1.5 – 2
446 hours with Dynabeads Protein G beads (Invitrogen™; Cat. No. 10004D), preblocked with 1
447 mg/ml BSA and 0.3 mg/ml Salmon Sperm DNA (Invitrogen™; Catalog No. AM9680). The beads
448 were then washed 2x with ChIP lysis buffer I, 2x with high salt ChIP wash buffer (50 mM HEPES
449 pH 7.5, 500 mM NaCl, 1 mM EDTA, 1% Triton X-100, 0.1% Na-deoxycholate), 2x with ChIP

450 wash buffer (10 mM Tris-HCl pH 8.0, 0.25 M LiCl, 0.5% NP-40, 0.5% Na-deoxycholate, 1 mM
451 EDTA), and 1x with 1x TE buffer (10 mM Tris-HCl pH 8.0, 1 mM EDTA). After washing, the
452 suspension was centrifuged at 1700 x g for 20 – 30 seconds. Protein-DNA complexes were
453 eluted from the beads with 1x ChIP elution buffer (50 mM Tris-HCl pH 8.0, 1% SDS, 1mM EDTA)
454 by incubating at 65°C for 20 – 30 minutes with occasional vortexing. To reverse the protein-DNA
455 crosslinks, the suspension was incubated overnight at 65°C with 0.2 M NaCl. The non-
456 crosslinked suspension was treated with 1 µg of RNase A (Thermo Scientific™; Catalog No.
457 FEREN0531) at 37°C for 30 minutes and with 0.8 units of Proteinase K (Thermo Scientific™;
458 Catalog No. FEREO0491) at 45°C for 45 minutes. The DNA was purified using the QIAquick
459 PCR Purification Kit (Qiagen; Catalog No. 28106) according to the manufacturer's protocol. The
460 purified DNA was subjected to either qPCR with Radiant™ Green qPCR Master Mix (2x) (Alkali
461 Scientific; Catalog No. QS1001) in 384-well plates or library preparation for sequencing.
462
463 **Chromatin immunoprecipitation in human cells.** ChIP-qPCR experiments were done as
464 described previously [37]. Briefly, HCT116 cells grown to 50-60% confluence were crosslinked with
465 1% formaldehyde for 10 minutes at 25°C. Crosslinking was quenched with 125 mM glycine for 5
466 minutes at 25°C. Cells were washed twice with ice-cold PBS and collected into 1 ml of RIPA
467 (150 mM NaCl, 1% v/v Nonidet P-40, 0.5% w/v deoxycholate, 0.1% w/v SDS, 50 mM Tris pH
468 8.0, 5 mM EDTA) buffer supplemented with protease and phosphatase inhibitors for each 150-
469 mm dish. Cells were lysed, and chromatin was sheared by sonication in a Bioruptor at high
470 power, for 3 x 10 minutes with cycles of 30 seconds ON and 30 seconds OFF. Lysates were
471 clarified by centrifugation at 20,000 x g for 20 minutes at 4°C. Before immunoprecipitation,
472 lysates (~5 x 10^6 cells per experiment) were pre-cleared with Pierce™ Protein A Agarose
473 (Thermo Scientific™; Catalog No. PI20333) for 2 hours at 4°C. Beads were separated by
474 centrifugation at 4000 x g for 1 minute at 4°C. The resulting supernatant was incubated with anti-
475 Cdk9 antibody (Abclonal; Catalog No. A11145) and Pol II (D8L4Y) (Cell Signaling Technology;

476 Catalog No. 14958S) for 4 hours at 4°C with constant nutation. The suspension was incubated
477 at 25°C for an additional 2 hours with Dynabeads Protein G beads, pre-blocked with 1 mg/ml
478 BSA and 0.25 mg/ml Salmon Sperm DNA. The beads were washed 2x with RIPA buffer, 4x with
479 Szak IP wash buffer (100 mM Tris-HCl, pH 8.5, 500 mM lithium chloride, 1% (v/v) nonidet-P-40,
480 1% (w/v) sodium deoxycholate), 2x with RIPA buffer, and 2x with TE buffer. After all wash steps,
481 centrifugation was performed at 1700 x g for 1 minute at 4°C. Protein-nucleic acid complexes
482 were eluted from the beads with elution buffer (46 mM Tris-HCl, pH 8.0, 0.65 mM EDTA, 1%
483 SDS) by incubating at 65°C for 15 minutes with occasional vortexing. Crosslinking was reversed
484 by incubating at 65°C for 16 hours. The un-crosslinked suspension was treated with 1 µg of
485 RNase A at 37°C for 30 minutes and with 0.8 units of Proteinase K at 45°C for 45 minutes. DNA
486 was purified using the QIAquick® PCR Purification Kit according to the manufacturer's protocol.
487 The purified DNA was subjected to either qPCR or library preparation for sequencing.
488
489 **ChIP-seq analysis.** Multiplexed ChIP-seq libraries were prepared using the NEBNext® Ultra™
490 II DNA Library Preparation kit (E7103S) with 25-50 ng of input or IP DNA and barcode adaptors
491 (NEBNext Multiplex Oligos for Illumina [Set 1, E7335] & [Set 2, E7500]). 150-nucelotides (150-
492 nt) paired-end sequencing (PE150) was performed on NovaSeq 6000. Quality control and
493 adapter trimming of FASTQ (raw sequencing) files were done in Galaxy using FastQC Read
494 Quality reports (Galaxy Version 0.74) and Trimmomatic flexible read trimming tool for Illumina
495 NGS data (Galaxy Version 0.39), respectively. Processed FASTQ files were aligned to the *S.*
496 *pombe* or human genome (version hg19) using Bowtie2[38] (Galaxy Version 2.5.3). Aligned
497 sequences of each biological replicate were fed into MACS2[39] (Galaxy Version 2.2.9.1) to call
498 peaks from alignment results. Generated "bedgraph treatment" files were converted to bigwig
499 using "Convert BedGraph to BigWig" (Galaxy Version 1.0.1), mean signal was computed using
500 "bigwigCompare" (Galaxy Version 3.5.4). Generated bigwig files were processed using
501 computeMatrix (Galaxy Version 3.5.4) in DeepTools[40] to prepare data for plotting heatmaps and/

502 or profiles of given regions. Heatmap and Metagene plots were generated using “plot Heatmap”
503 (Galaxy Version 3.5.4) and “plotProfile” (Galaxy Version 3.5.4) tools, respectively. The $\log_2$
504 signal ratios were calculated using “bigwigCompare” (Galaxy Version 3.5.4).
505
506 **Quantitative RT-PCR (RT-qPCR).** *S. pombe* cell cultures (50 mL) of strains JS78 (WT), LV259
507 (*htb1-K119R*), and TB4 (*ubp8D*) were grown to OD_{600} of 0.5. Total RNA was extracted by a hot
508 phenol method [41] and further purified on Qiagen RNeasy columns. For strand-specific RT-qPCR
509 to measure levels of *psu1*$^+$, *pgk1*$^+$, *pyk1*$^+$ and *pho1*$^+$ transcripts, 1 µg total RNA was converted to
510 cDNA using the superscript III kit (Invitrogen) and gene-specific primers listed in Extended Data
511 Table 2. Expression levels were normalized to those of the 18sDNA transcript in each strain.
512
513 **Data Access**
514 The raw and processed sequencing files have been submitted to the NCBI Gene Expression
515 Omnibus (GEO; https://www.ncbi.nlm.nih.gov/geo/query/acc.cgi) (Accession number:
516 GSE271342). The published data used in this study under the following accession code:
517 GSE115682 [16] and GSE138548 [42].

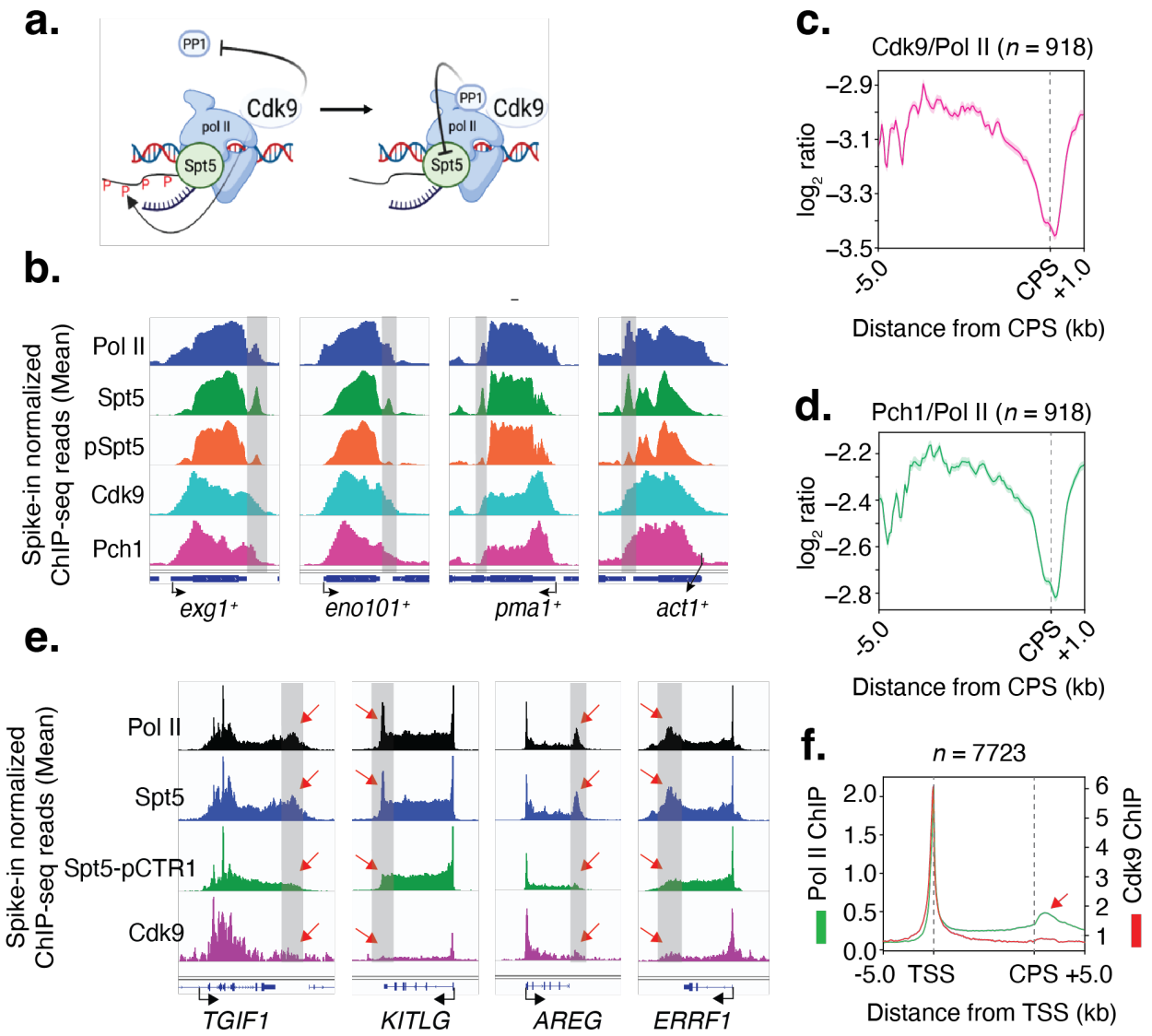

Figure 1 | Cdk9 and Pch1 dissociate from the elongation complex when Pol II passes the CPS. a, The model shows the Cdk9-PP1 switch controlling the transition from elongation to termination (PP1, protein phosphatase 1). The figure is prepared using (https://www.biorender.com/). **b**, In fission yeast, Cdk9 and Pch1 leave the elongation complex during the transition to termination. Individual gene tracks show that Cdk9 and Pch1 occupancy drops downstream of the CPS at the Pol II 3'-pause site (indicated by a gray shade). At the same location, Spt5 accumulates while Spt5 phosphorylation (pSpt5) decreases. **c**, **d**, Genome-wide distribution of Cdk9 and Pch1 on 1 kb separated genes (*n* = 918). Metagene analyses

527 reveal a sharp drop in Cdk9 and Pch1 occupancy when Pol II approaches the CPS (marked by
528 a vertical dotted line). Genes were sorted based on region length between -5 kb to +1 kb
529 relative to the CPS. The mean $\log_2$ ratio over Pol II was plotted in the summary image. **e**, In
530 humans, Cdk9 releases from the elongation complex after the CPS. Representative gene tracks
531 show that Cdk9 occupancy decreases downstream of the CPS where the Pol II 3'-pause peak is
532 positioned (indicated by a gray shade). At the same location, Spt5 accumulates while Spt5-
533 CTR1 phosphorylation (Spt5-pCTR1) decreases. Pol II, Spt5, and Spt5-pCTR1 ChIP data
534 utilized in this analysis were obtained from a published study [42]. Peaks are indicated by a red
535 arrow. **f**, Genome-wide distribution of Cdk9 and Pol II on 10 kb separated genes (*n* = 7723).
536 Metagene analyses reveal reduced levels of Cdk9 occupancy downstream of the CPS where
537 Pol II accumulates (indicated by a red arrow). Genes were sorted based on Pol II occupancy.
538 (Note: In this representation, the regions between the TSS and the CPS have been scaled to
539 enable comparisons among genes of different lengths.) The TSS and CPS are marked by
540 vertical dotted lines.
541

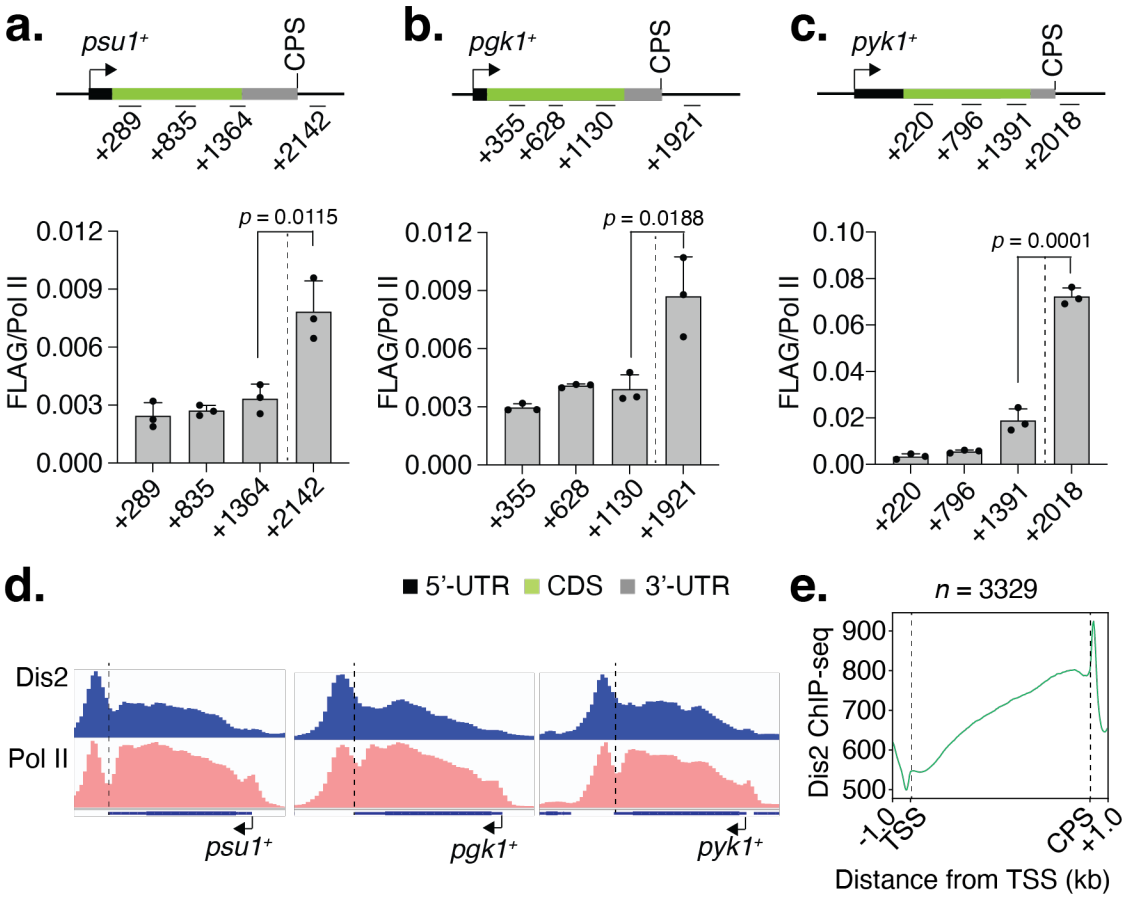

Figure 2 | Dis2 accumulates beyond the CPS. a-c, Dis2 ChIP was performed using chromatin extract from *S. pombe* cells expressing Dis2-FLAG, which is a C-terminal FLAG-tagged version of Dis2. ChIP-qPCR analyses show the distribution of Dis2 on *psu1*$^+$, *pgk1*$^+$, and *pyk1*$^+$ genes. The results reveal a sharp increase in Dis2 occupancy beyond the CPS at the location of the fourth amplicon. In the schematic diagram of genes, the 5'-untranslated region (5'-UTR), the coding sequence (CDS), and the 3'-UTR are demarcated by black, green, and gray, respectively. The regions of the genes scanned are indicated by amplicon positions. The experiments were performed with three biological replicates; one-sided error bars show standard deviation (s.d.) of mean; *p*-values (Student's *t*-test) are indicated in the plots between third (upstream of the CPS) and fourth (downstream of the CPS) amplicons. **d**, ChIP-seq browser tracks show the distribution of Dis2 and Pol II across *psu1*$^+$, *pgk1*$^+$, and *pyk1*$^+$ genes. The results show accumulation of Dis2 after the CPS corresponding to the position where Pol II

accumulates. **e**, Metagene analyses show a sharp accumulation of Dis2 beyond the CPS of Pol II-transcribed genes (*n* = 3329). In this plot, the regions between the TSS and the CPS have been scaled to enable comparisons among genes of different lengths. Vertical dotted lines mark the TSS and CPS.

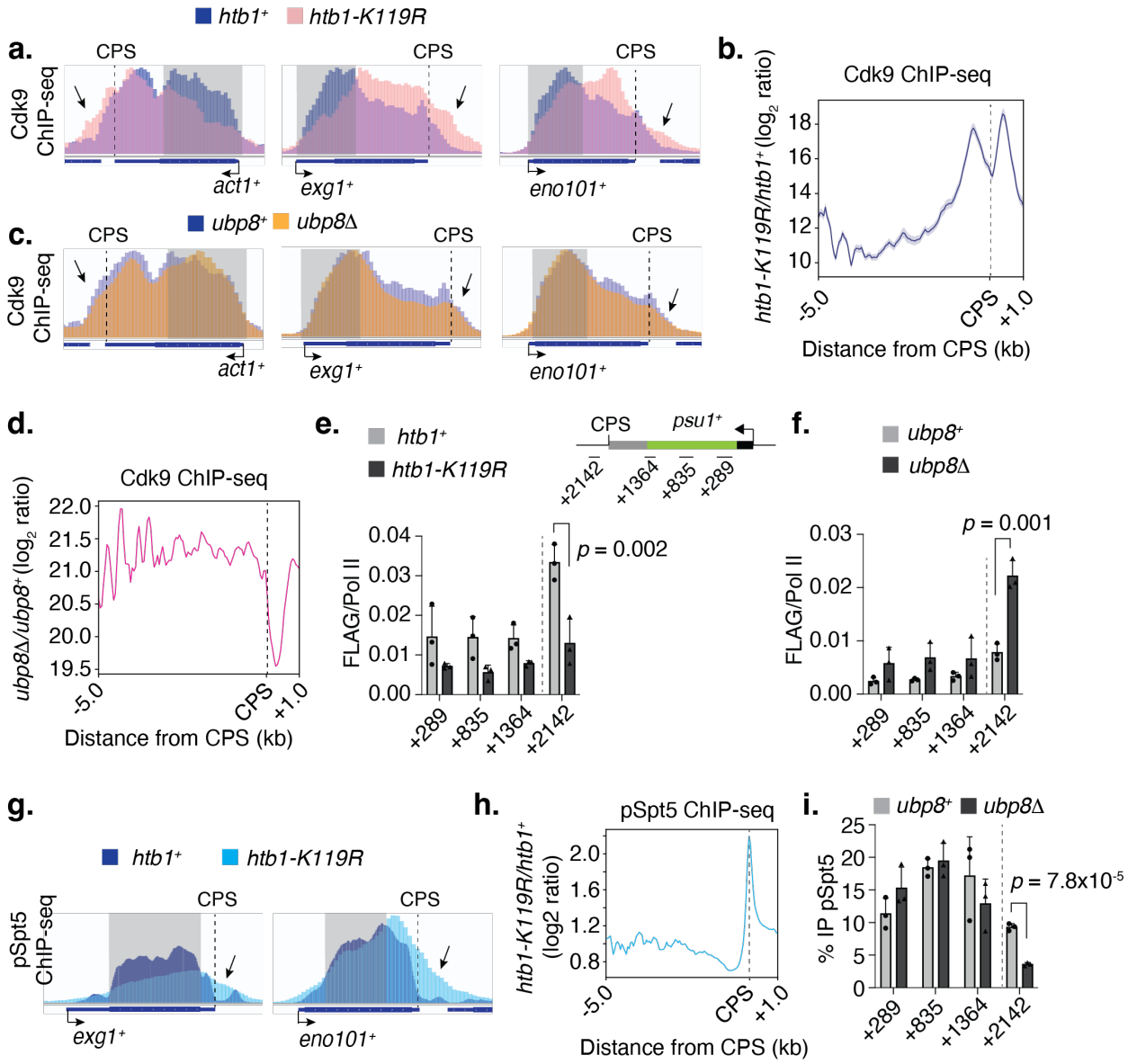

Figure 3 | H2Bub1 regulates Cdk9's chromatin occupancy. **a**, H2Bub1 differentially regulates Cdk9's chromatin occupancy throughout the transcription cycle. Individual browser tracks display an increase in Cdk9 occupancy downstream of the CPS (marked by an arrow)

564 and a decrease at the 5' end (marked by a gray shaded area) of the example genes upon loss
565 of H2Bub1. Cdk9 ChIP-seq was performed in cells expressing 13Myc-tagged Cdk9 in the *htb1*$^+$
566 and *htb1-K119R* backgrounds using an anti-Myc antibody. Blue and pink tracks represent the
567 Cdk9 distribution in *htb1*$^+$ and *htb1-K119R* cells, respectively, overlaid. **b**, The metagene plot
568 shows the genome-wide distribution of Cdk9 on 1 kb separated genes (n = 918) from -5.0 to
569 +1.0 kb relative to the CPS. Results indicate accumulation of Cdk9 upstream and downstream
570 of the CPS in *htb1-K119R* cells. The $\log_2$ ratio of mean ChIP-seq values in *htb1-K119R* over
571 *htb1*$^+$ is plotted. **c**, Similar to panel **a**, but Cdk9-13Myc ChIP was conducted in *ubp8*$^+$ and *ubp8Δ*
572 cells. Browser tracks reveal minimal changes in Cdk9 distribution at the 5' end (indicated by a
573 gray shaded area) of genes, but a decrease beyond the CPS (indicated by an arrow) in *ubp8Δ*
574 cells. Blue and orange tracks represent the Cdk9 distribution in *ubp8*$^+$ and *ubp8Δ* cells,
575 respectively, overlaid. **d**, The metagene plot shows the genome-wide distribution of Cdk9 on 1
576 kb separated genes (n = 918) from -5.0 to +1.0 kb relative to the CPS. Results indicate a rapid
577 drop of Cdk9 downstream of the CPS. The $\log_2$ ratio of mean ChIP-seq values in *ubp8Δ* over
578 *ubp8*$^+$ is plotted. **e**, ChIP-qPCR analyses show the distribution of Dis2-FLAG on the *psu1*$^+$ gene
579 in *htb1*$^+$ (gray bar) and *htb1-K119R* (black bar) cells. Results indicate a significant decrease in
580 Dis2 occupancy after the CPS in *htb1-K119R* cells. **f**, ChIP-qPCR analyses show the distribution
581 of Dis2-FLAG on the *psu1*$^+$ gene in *ubp8*$^+$ (gray bar) and *ubp8Δ* (black bar) cells. Results
582 indicate a significant increase in Dis2 occupancy after the CPS in *ubp8Δ* cells. For **e**, **f**,
583 experiments were performed in cells expressing Dis2 as C-terminal FLAG tagged; graphs
584 plotted the ratio of Dis2-FLAG ChIP over Pol II along the Y-axis. **g**, Similar to panel **a**, but pSpt5
585 ChIP-seq was conducted in *htb1*$^+$ and *htb1-K119R* cells. Individual browser tracks display an
586 increase in pSpt5 occupancy downstream of the CPS (marked by an arrow) and a decrease at
587 the 5' end (marked by a gray shaded area) of the example genes upon loss of H2Bub1. Blue
588 and cyan tracks represent the pSpt5 distribution in *htb1*$^+$ and *htb1-K119R* cells, respectively,
589 overlaid. **h**, The metagene plot shows the genome-wide distribution of pSpt5 on 1 kb separated

590 genes (*n* = 918) from -5.0 to +1.0 kb relative to the CPS. Results indicate accumulation of pSpt5
591 around the CPS in *htb1-K119R* cells. The $\log_2$ ratio of mean ChIP-seq values in *htb1-K119R*
592 over *htb1*$^+$ is plotted. **i**, ChIP-qPCR analyses show the distribution of pSpt5 on the *psu1*$^+$ gene in
593 *ubp8*$^+$ (gray bar) and *ubp8Δ* (black bar) cells. Results indicate a significant decrease in pSpt5
594 occupancy after the CPS in *ubp8Δ* cells. For panels **e**, **f**, and **i**, experiments were performed
595 with three independent biological replicates (*n* = 3); one-sided error bars show the standard
596 deviation (s.d.) of mean ChIP values; *p*-values (Student's t-test) are indicated in the plots. For
597 panels **a**-**i**, vertical dotted lines mark the CPS.
598

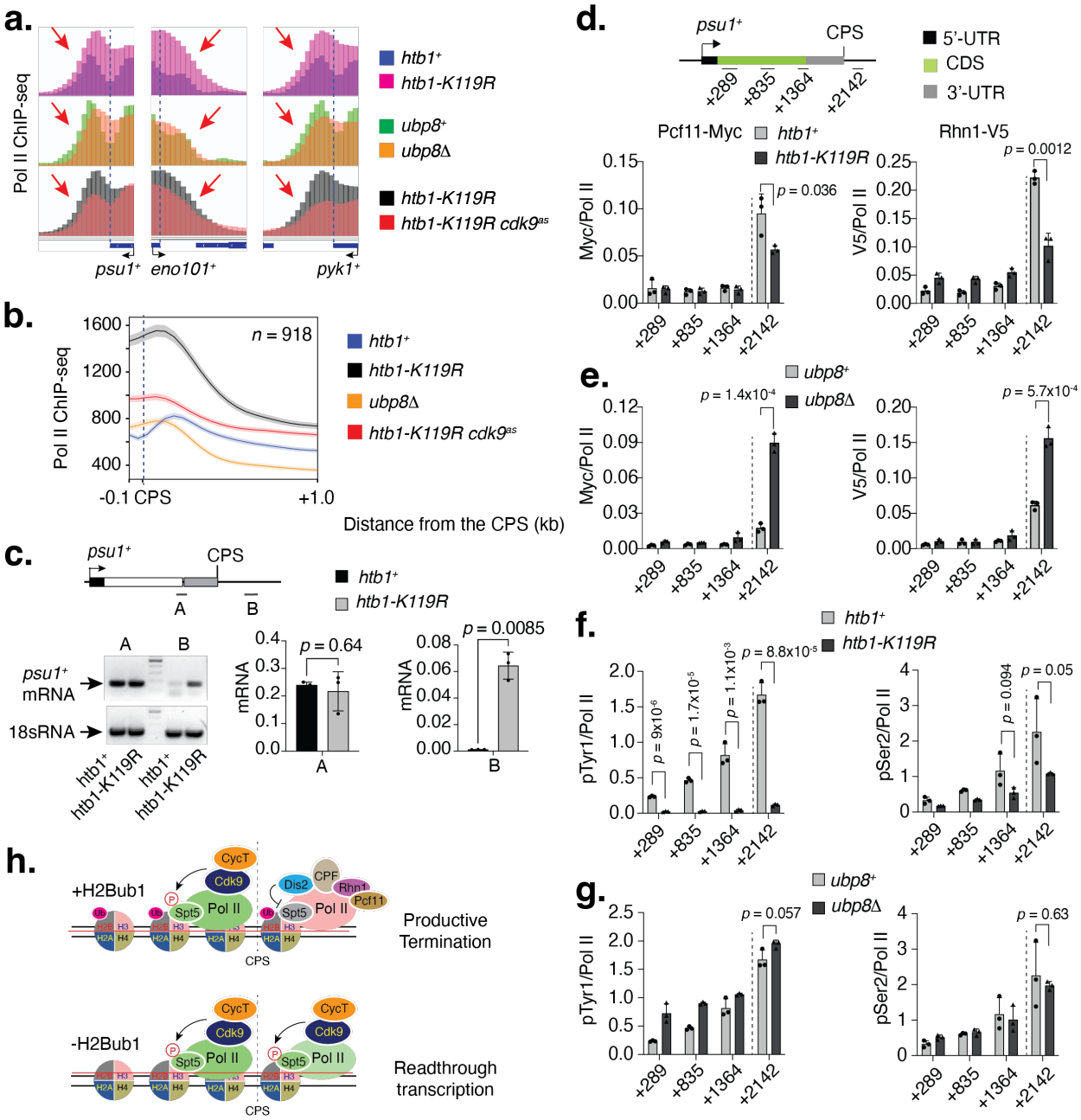

Figure 4 | H2Bub1 controls termination. a, Loss of H2Bub1 impairs termination. ChIP-seq browser tracks reveal an extended Pol II distribution in *htb1-K119R* cells beyond the regular termination zone seen in *htb1*$^{+}$ cells, indicating readthrough transcription, i.e., termination defects. The blue and pink tracks, representing the Pol II distribution in *htb1*$^{+}$ and *htb1-K119R* cells, respectively, are overlaid. Conversely, persistent levels of H2Bub1 favor termination. ChIP-seq browser tracks show a narrowed Pol II distribution in the termination zone in *ubp8Δ*

606 cells, indicating that hyper mono-ubiquitylation favors termination. The green and orange tracks,
607 representing the Pol II distribution in *ubp8*$^{+}$ and *ubp8Δ* cells, respectively, are overlaid. Cdk9
608 inhibition in the *htb1-K119R* background narrows Pol II distribution, suggesting a rescue of
609 termination defects. This indicates that the accumulation of Cdk9 following the loss of H2Bub1 is
610 the main trigger for termination defects by continuing elongation. The black and red tracks,
611 representing the Pol II distribution in *htb1-K119R*, with or without inhibition of Cdk9, respectively,
612 are overlaid. Pol II ChIP-seq data following Cdk9 inhibition in *htb1-K119R* cells, used in this
613 analysis, were obtained from a published study [16]. The regions of alterations in Pol II distribution
614 after the CPS are indicated by red arrows. The vertical dotted lines mark the CPS. **b**, The
615 metagene plot shows the genome-wide distribution of Pol II on 1 kb separated genes (*n* = 918)
616 from -0.1 kb to +1.0 kb relative to the CPS. Results indicate a broadening of Pol II distribution in
617 the termination zone in *htb1-K119R* cells, implying termination defects. Conversely, in *ubp8Δ*
618 cells, the Pol II distribution narrowed compared to wildtype (*ubp8*$^{+}$) cells, indicating premature
619 termination. Cdk9 [16] inhibition in the *htb1-K119R* background narrows Pol II distribution,
620 indicating a rescue of termination defects. The $\log_2$ ratio of mean ChIP-seq values in *htb1-*
621 *K119R* (or *ubp8Δ*) with active or inactive Cdk9 over wildtype (*htb1*$^{+}$/*ubp8*$^{+}$) is plotted. **c**, The left
622 panel shows an agarose gel visualizing transcript production from the upstream (A) and
623 downstream (B) regions of the CPS of the *psu1*$^{+}$ gene. The results indicate the synthesis of
624 *psu1*$^{+}$ mRNA beyond the regular termination zone in *htb1-K119R* cells, with little to no mRNA
625 synthesis in *htb1*$^{+}$ cells. The right panel shows RT-qPCR analyses quantifying *psu1*$^{+}$ mRNA
626 production from the same regions, A and B, indicating increased mRNA synthesis beyond the
627 termination zone in *htb1-K119R* cells. For panel **c**, individual data points shown in the plots were
628 obtained from three independent biological replicates (*n* = 3); two-sided error bars represent the
629 standard deviation (s.d.) of mean qRT-PCR values; *p*-values (Student's t-test) are indicated in
630 the plots. **d**, Loss of H2Bub1 impairs the recruitment of termination factors. ChIP-qPCR
631 analyses reveal a significant decrease in the recruitment of termination factors, Pcf11-Myc and

632 Rhn1-V5, after the CPS of *psu1*$^{+}$ in *htb1-K119R* cells. **e**, Persistent levels of H2Bub1 facilitate
633 termination factor recruitment. ChIP-qPCR analyses show a significant increase in the
634 recruitment of Pcf11 and Rhn1 beyond the CPS of *psu1*$^{+}$ gene in *ubp8Δ* cells. **f**, ChIP-qPCR
635 analyses demonstrate a significant reduction of Pol II CTD phosphorylation at Tyr1 and Ser2 in
636 *htb1-K119R* cells. **g**, ChIP-qPCR analyses illustrate little to no changes in Tyr1 and Ser2
637 phosphorylation of Pol II CTD in *ubp8Δ* cells. For panels **c**-**g**, experiments were performed with
638 three independent biological replicates (n = 3); one-sided error bars represent the standard
639 deviation (s.d.) of mean qRT-PCR values. p-values (Student's t-test) are indicated in the plots.
640 **h**, A model for elongation to termination suggests that proper levels of H2Bub1 cause Cdk9 to
641 dissociate from the elongation complex. This dissociation allows the recruitment of cleavage
642 and polyadenylation factor (CPF)-associated Dis2, which dephosphorylates Spt5, signaling Pol
643 II to slow down. Slow Pol II leads to the accumulation of Pol II CTD phosphorylation (pTyr1 and
644 pSer2), which facilitates the recruitment of termination factor, Pcf11 and Rhn1. However, when
645 H2Bub1 is absent, Cdk9 remains associated with the elongation complex, preventing the
646 recruitment of CPF-Dis2. As a result, high levels of phosphorylated Spt5 (pSpt5) persist,
647 promoting active elongation and leading to read-through transcription. The CPS is marked by
648 dotted lines.
649
650
651

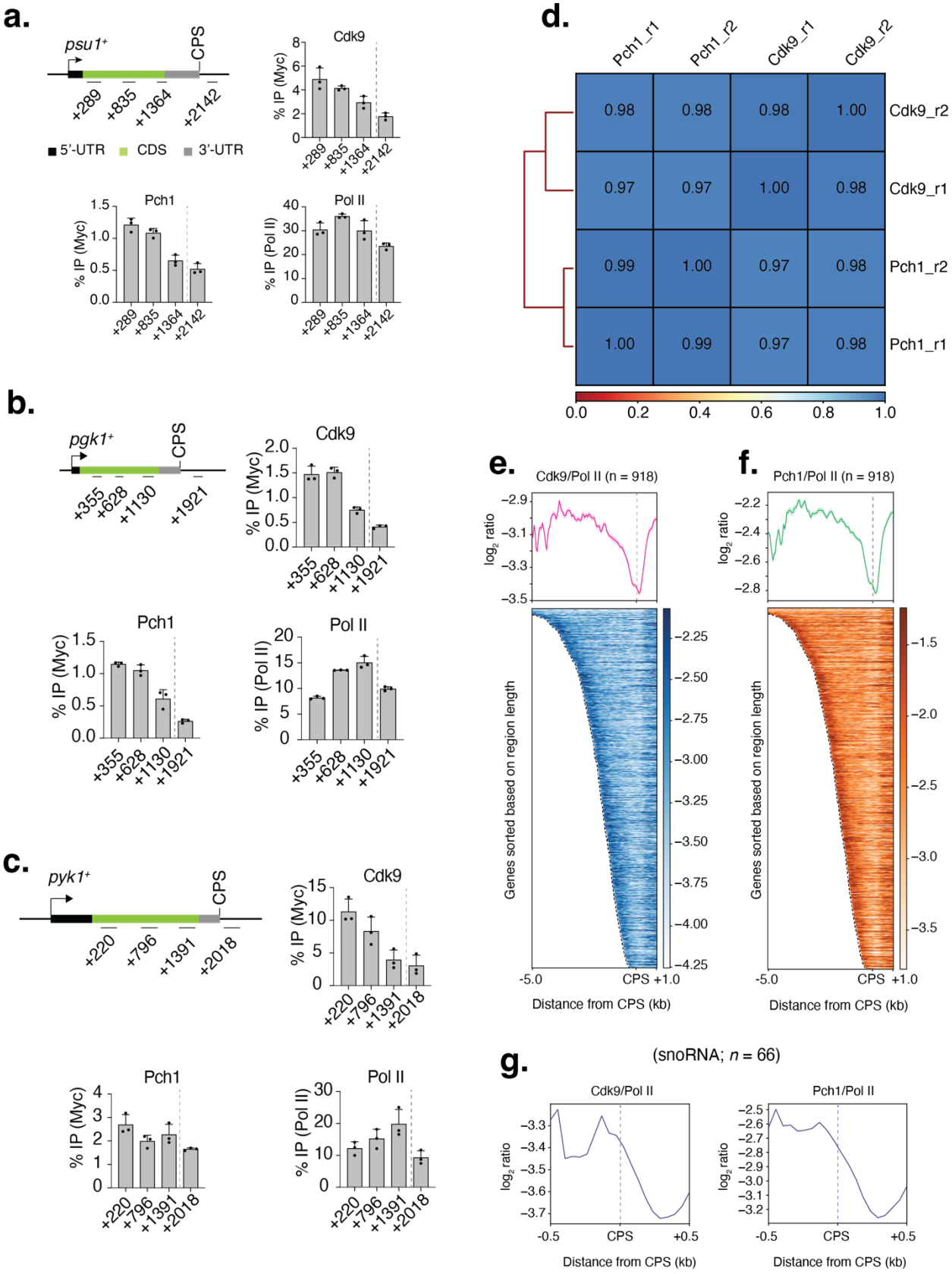
a.
psu1+
CPS
+289
+835
+1364
+2142
5'-UTR
CDS
3'-UTR
Cdk9
Pch1
Pol II
% IP (Myc)
% IP (Pol II)
b.
pgk1+
+355
+628
+1130
+1921
c.
pyk1+
+220
+796
+1391
+2018
d.
Pch1_r1
Pch1_r2
Cdk9_r1
Cdk9_r2
0.98 0.98 0.98 1.00
0.97 0.97 1.00 0.98
0.99 1.00 0.97 0.98
1.00 0.99 0.97 0.98
e.
Cdk9/Pol II (n = 918)
f.
Pch1/Pol II (n = 918)
log2 ratio
Genes sorted based on region length
Distance from CPS (kb)
g.
(snoRNA; n = 66)
Cdk9/Pol II
Pch1/Pol II

652

653 **Extended Data Figure 1 | Release of Cdk9 and Pch1 from the elongation complex in**
654 **fission yeast when Pol II traverses the CPS**. **a**, ChIP-qPCR analyses show a gradual
655 decrease in the occupancy of Cdk9 and Pch1 towards the 3'-end of the *psu1*$^+$ gene. **b**, ChIP-
656 qPCR analyses show a gradual decrease in the occupancy of Cdk9 and Pch1 towards the 3'-
657 end of the *pgk1*$^+$ gene. **c**, ChIP-qPCR analyses show a gradual decrease in the occupancy of
658 Cdk9 and Pch1 towards the 3'-end of the *pyk1*$^+$ gene. For panels **a**-**c**, individual data values
659 were obtained from three (n = 3) independent experiments; one-sided error bars represent the
660 standard deviation (s.d.) of mean ChIP values. **d**, Correlation between ChIP-seq samples.
661 Paired-end sequencing reads were mapped to the fission yeast genome using Bowtie2 (Galaxy
662 Version 2.5.3+galaxy1). Mapped reads of each biological replicate were used to calculate the
663 correlation between pairs of replicates. Values in boxes represent the Pearson correlation
664 coefficient between corresponding samples (n = 2 biological replicates). **e**, Genome-wide
665 distribution of Cdk9. Metagene analyses (top) and heatmaps (bottom) show a comparison
666 between $\log_2$ ratios of Cdk9:Pol II for Pol II-transcribed genes (1 kb separated; n = 918). **f**,
667 Genome-wide distribution of Pch1. Metagene analyses (top) and heatmaps (bottom) show a
668 comparison between $\log_2$ ratios of Pch1:Pol II for Pol II-transcribed genes (1 kb separated; n =
669 918). For panels **e** and **f**, genes were sorted based on region length between -5 kb to +1 kb
670 relative to the CPS. **g**, Distribution of Cdk9 and Pch1 on snoRNA genes. Metagene analyses
671 show genome-wide comparison between $\log_2$ ratios of Cdk9:Pol II or Pch1:Pol II for Pol II-
672 transcribed snoRNA genes (n = 66) from -0.5 kb to +0.5 kb relative to the CPS. The CPS is
673 marked by vertical dotted lines.
674

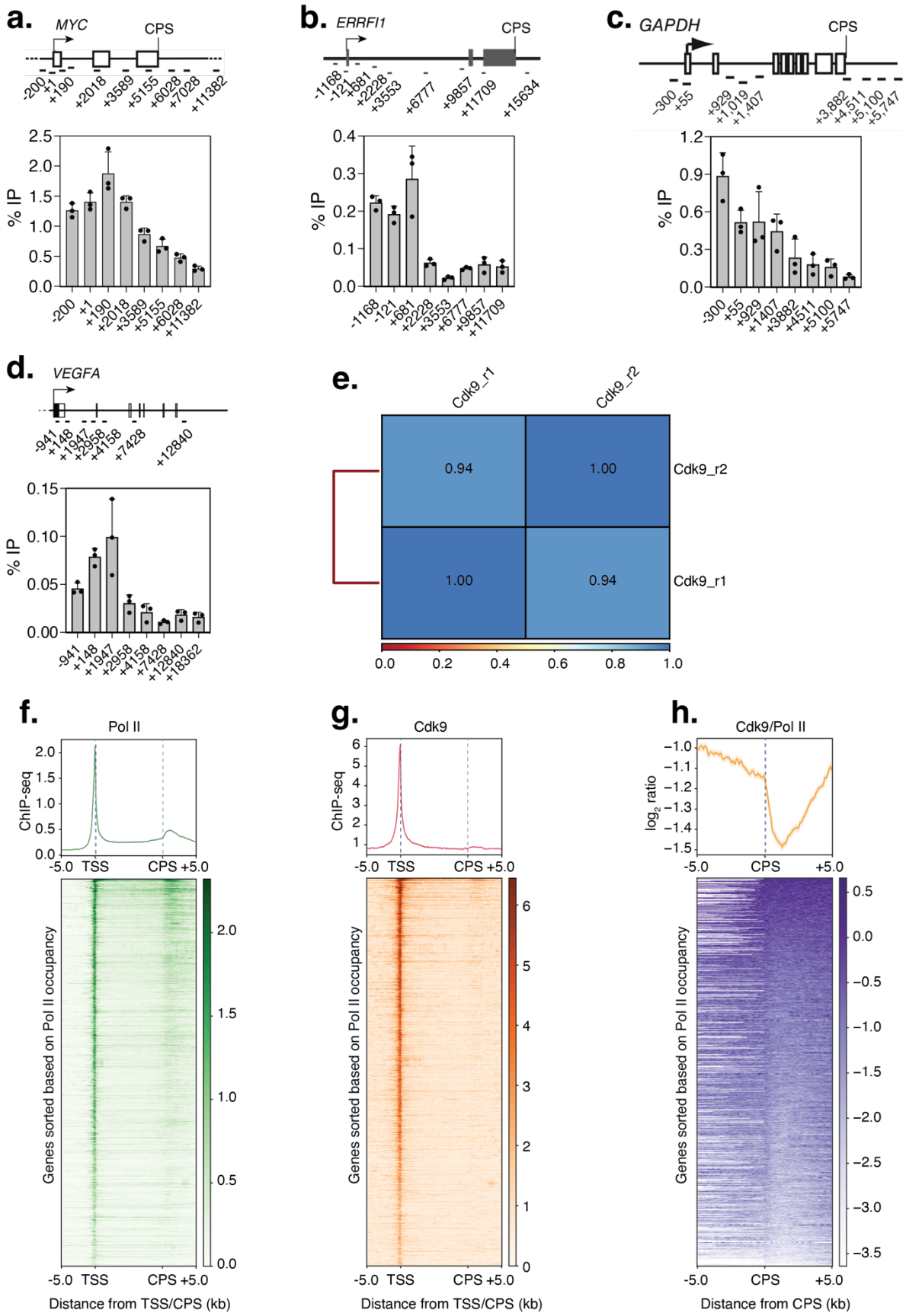
a.
MYC
CPS
-200
+1
+190
+2018
+3589
+5155
+6028
+7028
+11382
% IP
b.
ERRFI1
CPS
-1168
-121
+681
+2228
+3553
+6777
+9857
+11709
+15634
c.
GAPDH
CPS
-300
+55
+929
+1,019
+1,407
+3,882
+4,511
+5,100
+5,747
d.
VEGFA
-941
+148
+1947
+2958
+4158
+7428
+12840
+18362
e.
Cdk9_r1
Cdk9_r2
0.94
1.00
1.00
0.94
f.
Pol II
ChIP-seq
-5.0 TSS
CPS +5.0
Genes sorted based on Pol II occupancy
Distance from TSS/CPS (kb)
g.
Cdk9
h.
Cdk9/Pol II
log2 ratio
-5.0
CPS
+5.0
Distance from CPS (kb)

675

676 **Extended Data Figure 2 | Cdk9 dissociation as Pol II crosses the CPS in human cells**. **a-d**,
677 ChIP-qPCR analyses show a gradual decrease in Cdk9 occupancy towards the 3'-end of *MYC*
678 (**a**), *ERRFI1* (**b**), *GAPDH* (**c**), and *VEGFA* (**d**). Individual data values in panels **a-d** were
679 obtained from three independent experiments (*n* = 3). One-sided error bars represent the
680 standard deviation (s.d.) of the mean ChIP values. **e**, Correlation between Cdk9 ChIP-seq
681 samples. Paired-end sequencing reads were mapped to the human genome (hg19) using
682 Bowtie2 (Galaxy Version 2.5.3+galaxy1). Mapped reads of each biological replicate were used
683 to calculate the correlation between pairs of replicates. Values in boxes represent the Pearson
684 correlation coefficient between corresponding samples (*n* = 2 biological replicates). **f**, Genome-
685 wide distribution of Pol II. Metagene analyses (top) and heatmaps (bottom) show the distribution
686 of Pol II. Pol II ChIP data utilized in this analysis were obtained from a published study [42]. **g**,
687 Genome-wide distribution of Cdk9. Metagene analyses (top) and heatmaps (bottom) show the
688 distribution of Cdk9. **h**, Genome-wide distribution of Cdk9 with a CPS-centered focus. Metagene
689 analyses (top) and heatmaps (bottom) display the distribution of Cdk9 on Pol II-transcribed
690 genes from -5.0 kb to +5.0 kb. The $\log_2$ ratios of Cdk9:Pol II were plotted. For **f**, **g**, the regions
691 between the TSS and the CPS have been scaled for comparison among genes of different
692 lengths. For **f-h**, plots were generated using 10 kb separated Pol II-transcribed genes (*n* =
693 7723). The TSS and CPS are marked by vertical dotted lines.
694

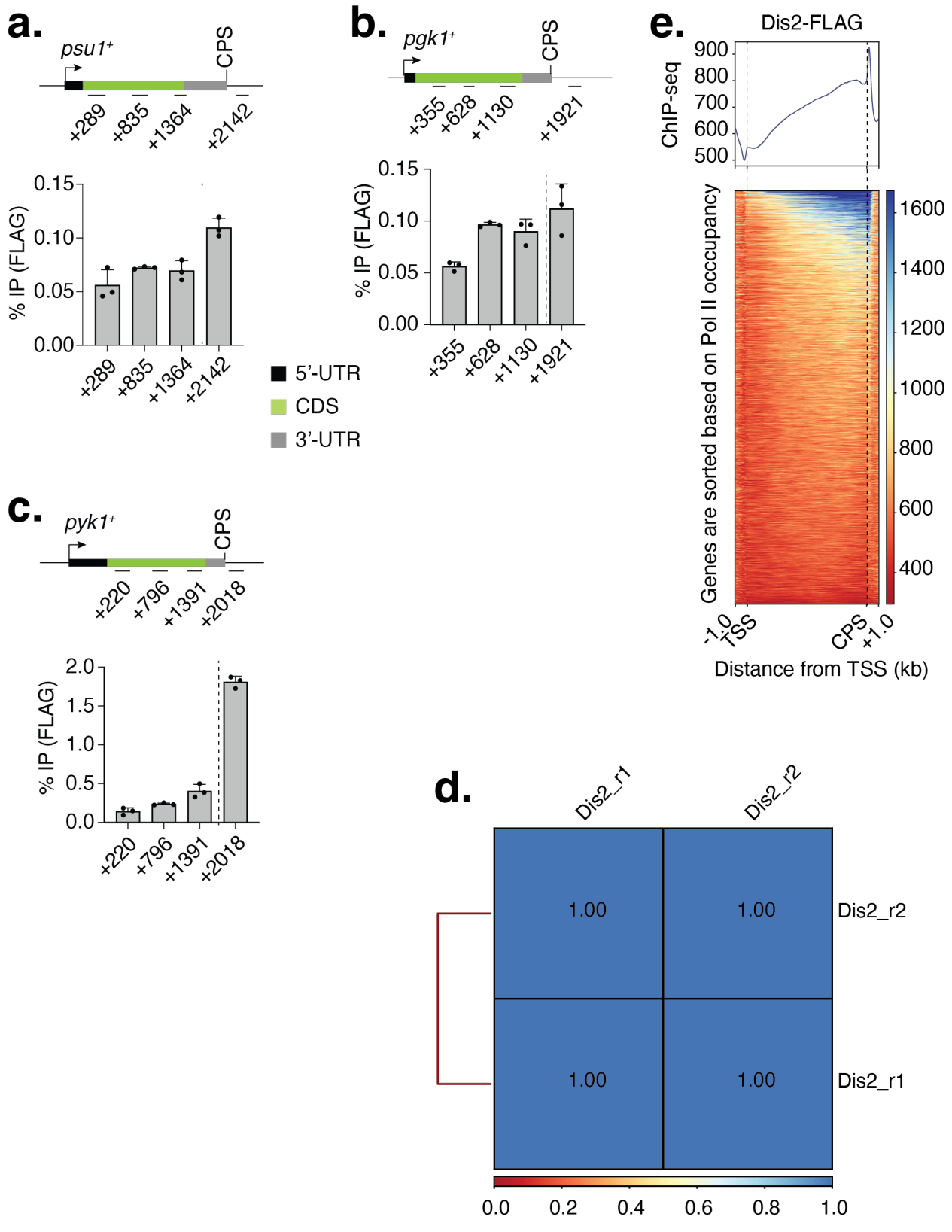
a.
psu1+
CPS
+289
+835
+1364
+2142
% IP (FLAG)
0.15
0.10
0.05
0.00
b.
pgk1+
CPS
+355
+628
+1130
+1921
c.
pyk1+
+220
+796
+1391
+2018
2.0
1.5
1.0
0.5
0.0
5'-UTR
CDS
3'-UTR
e.
Dis2-FLAG
ChIP-seq
900
800
700
600
500
Genes are sorted based on Pol II occupancy
1600
1400
1200
1000
800
600
400
-1.0
TSS
CPS
+1.0
Distance from TSS (kb)
d.
Dis2_r1
Dis2_r2
1.00
0.0
0.2
0.4
0.6
0.8
1.0

695

696 **Extended Data Figure 3 | Sharp accumulation of Dis2 after the CPS in fission yeast**
697 **genes**. **a**-**c**, ChIP-qPCR analyses show a gradual increase in Dis2 occupancy towards the 3'-
698 end of *psu1*$^{+}$ (**a**), *pgk1*$^{+}$ (**b**), and *pyk1*$^{+}$ (**c**) genes, with a sharp increase in occupancy after the
699 CPS (marked by vertical dotted lines). Experiments were performed with three biological
700 replicates (n = 3). Individual data points are shown in the plots. One-sided error bars represent
701 the standard deviation (s.d.) of the mean ChIP values. **d**, Correlation between Dis2-FLAG ChIP-
702 seq samples. Paired-end sequencing reads were mapped to the fission yeast genome using
703 Bowtie2 (Galaxy Version 2.5.3+galaxy1). Mapped reads of each biological replicate were used
704 to calculate the correlation between pairs of replicates. Values in boxes represent the Pearson
705 correlation coefficient between corresponding samples (n = 2 biological replicates). **e**, Genome-
706 wide distribution of Dis2. Metagene analyses (top) and heatmaps (bottom) demonstrate the
707 dramatic accumulation of Dis2 beyond the CPS of Pol II-transcribed genes (n = 7723). Genes
708 are sorted based on Pol II occupancy. The regions between the TSS and the CPS have been
709 scaled for comparison among genes of different lengths. The TSS and CPS are marked by
710 vertical dotted lines.
711

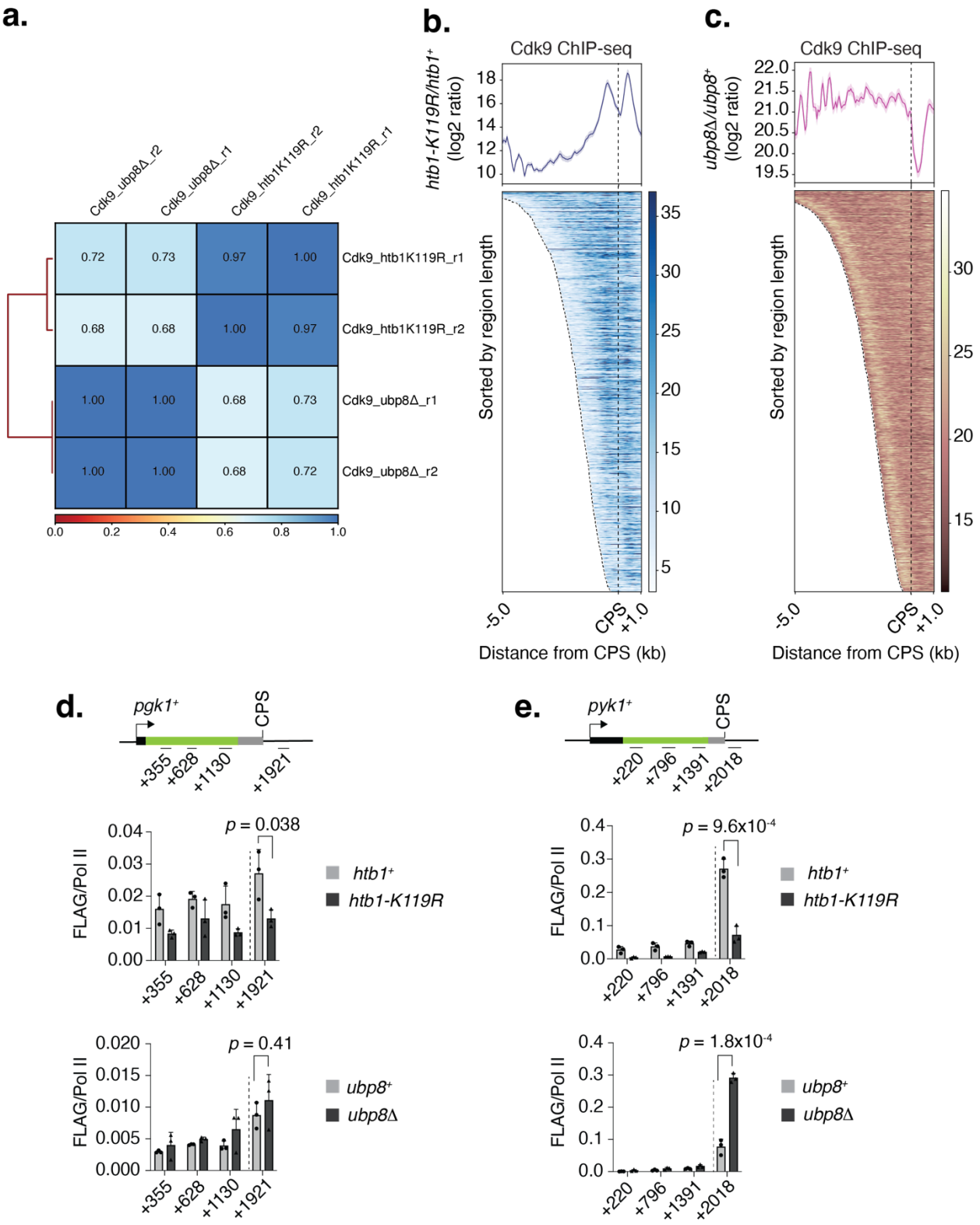

712

713 **Extended Data Figure 4 | H2Bub1 regulates the distribution of Cdk9 and Dis2**. **a**,

714 Correlation between ChIP-seq samples. Paired-end sequencing reads were mapped to the

715 fission yeast genome using Bowtie2 (Galaxy Version 2.5.3+galaxy1). The correlation between
716 pairs of replicates was calculated using mapped reads from each biological replicate. Values in
717 boxes represent the Pearson correlation coefficient between corresponding samples (n = 2
718 biological replicates). **b**, Genome-wide distribution of Cdk9 upon loss of H2Bub1. Metagene
719 analyses (top) and heatmaps (bottom) compare the $\log_2$ ratios of mean ChIP values in *htb1-*
720 *K119R* and *htb1*$^+$ for Pol II-transcribed genes (n = 918). **c**, Genome-wide distribution of Cdk9
721 under persistent levels of H2Bub1. Metagene analyses (top) and heatmaps (bottom) compare
722 the $\log_2$ ratios of mean ChIP values in *ubp8D* and *ubp8*$^+$ for Pol II-transcribed genes (n = 3329).
723 For **b**, **c**, genes were sorted based on region length between -5 kb to +1 kb relative to the CPS.
724 **d**, Distribution of Dis2 on *pgk1*$^+$ gene. ChIP-qPCR analyses show a significant decrease in Dis2
725 occupancy after the CPS (marked by a vertical dotted line) in *htb1-K119R* cells (top panel), with
726 a modest increase in *ubp8D* cells (bottom panel). **e**, Distribution of Dis2 on *pyk1*$^+$ gene. ChIP-
727 qPCR analyses reveal a significant decrease in Dis2 occupancy after the CPS (marked by a
728 vertical dotted line) in *htb1-K119R* cells (top panel). Conversely, Dis2 occupancy is increased in
729 *ubp8D* cells (bottom panel). For **d**,**e**, experiments were performed with three independent
730 biological replicates (n = 3); one-sided error bars show the standard deviation (s.d.) of mean
731 ChIP values; p-values (Student's t-test) are indicated in the plots; Y-axis show ratio plots of Dis2
732 ChIP over Pol II.
733

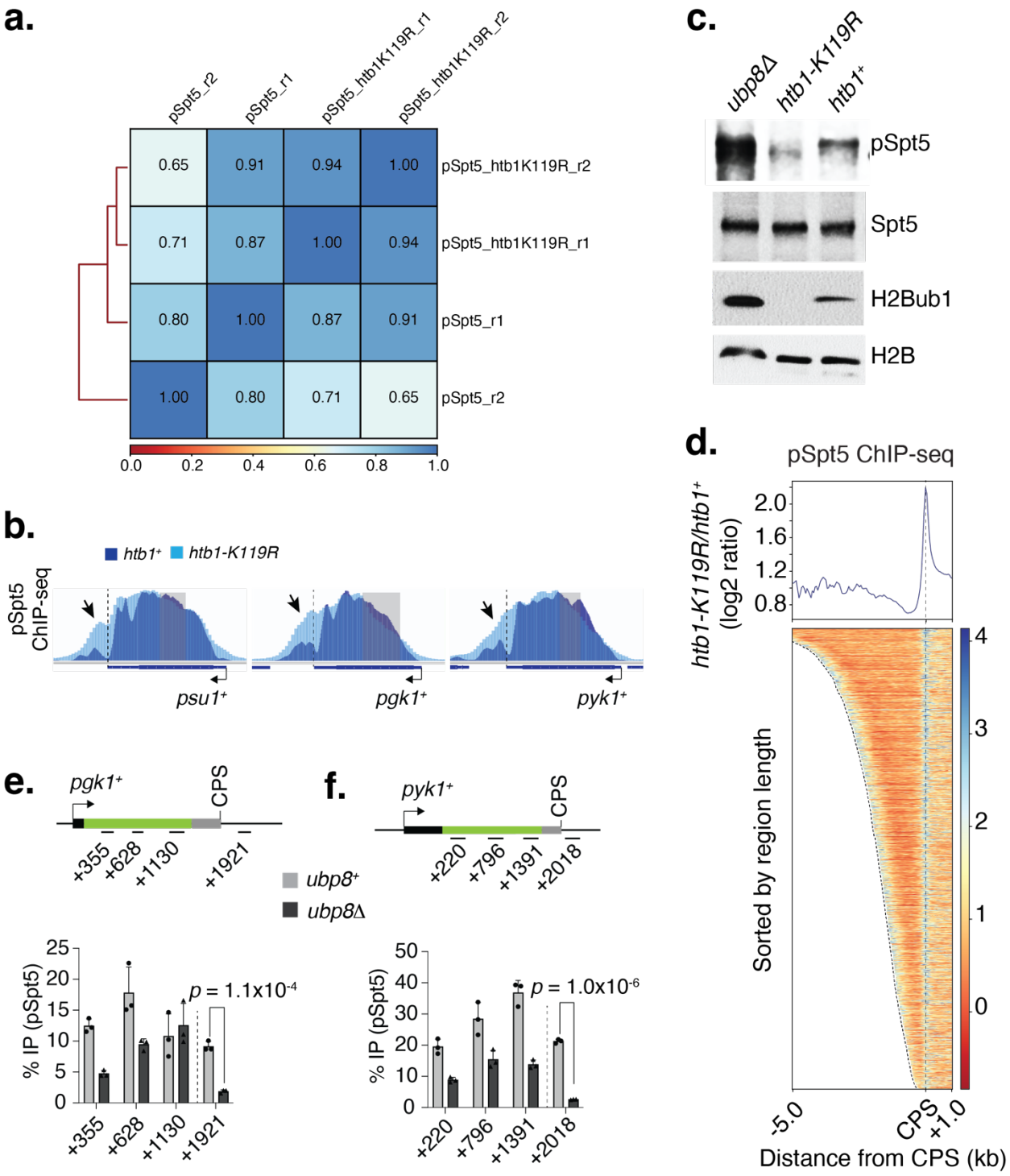

734

735 **Extended Data Figure 5 | H2Bub1 regulates Spt5 phosphorylation on chromatin**. **a**,

736 Correlation between ChIP-seq samples. Paired-end sequencing reads were mapped to the

737 fission yeast genome using Bowtie2 (Galaxy Version 2.5.3+galaxy1). The correlation between

738 pairs of replicates was calculated using mapped reads from each biological replicate. Values in
739 boxes represent the Pearson correlation coefficient between corresponding samples (*n* = 2
740 biological replicates). **b**, Individual browser tracks display an increase in pSpt5 occupancy
741 downstream of the CPS (marked by an arrow) and a decrease at the 5' end (marked by a gray
742 shaded area) of *psu1*$^+$, *pgk1*$^+$ and *pyk1*$^+$ upon loss of H2Bub1. Blue and cyan tracks represent
743 the pSpt5 distribution in *htb1*$^+$ and *htb1-K119R* cells, respectively, are overlaid. **c**, The
744 immunoblot shows a reduction in pSpt5 in the whole-cell extract of *htb1-K119R*, whereas it is
745 slightly stabilized in *ubp8Δ* cells. Additionally, there is a loss of H2Bub1 in *htb1-K119R* and a
746 slight increase in H2Bub1 in *ubp8Δ* cells. **d**, Genome-wide distribution of pspt5 upon loss of
747 H2Bub1. Metagene analyses (top) and heatmaps (bottom) compare the $\log_2$ ratios of mean
748 pSpt5 ChIP values in *htb1-K119R* and *htb1*$^+$ for Pol II-transcribed genes (*n* = 918). The genes
749 were sorted based on region length between -5 kb to +1 kb relative to the CPS. **e**, ChIP-qPCR
750 analyses show the distribution of pSpt5 on *pgk1*$^+$ gene in *ubp8*$^+$ (gray bar) and *ubp8Δ* (black
751 bar) cells. Results indicate a significant decrease in pSpt5 occupancy after the CPS in *ubp8Δ*
752 cells. **f**, ChIP-qPCR analyses show the distribution of pSpt5 on *pyk1*$^+$ gene in *ubp8*$^+$ (gray bar)
753 and *ubp8Δ* (black bar) cells. Results indicate a significant decrease in pSpt5 occupancy after
754 the CPS in *ubp8Δ* cells. For **e**,**f**, experiments were performed with three independent biological
755 replicates (*n* = 3); one-sided error bars show the standard deviation (s.d.) of mean ChIP values;
756 *p*-values (Student's t-test) are indicated in the plots. The vertical dotted lines mark the CPS.
757

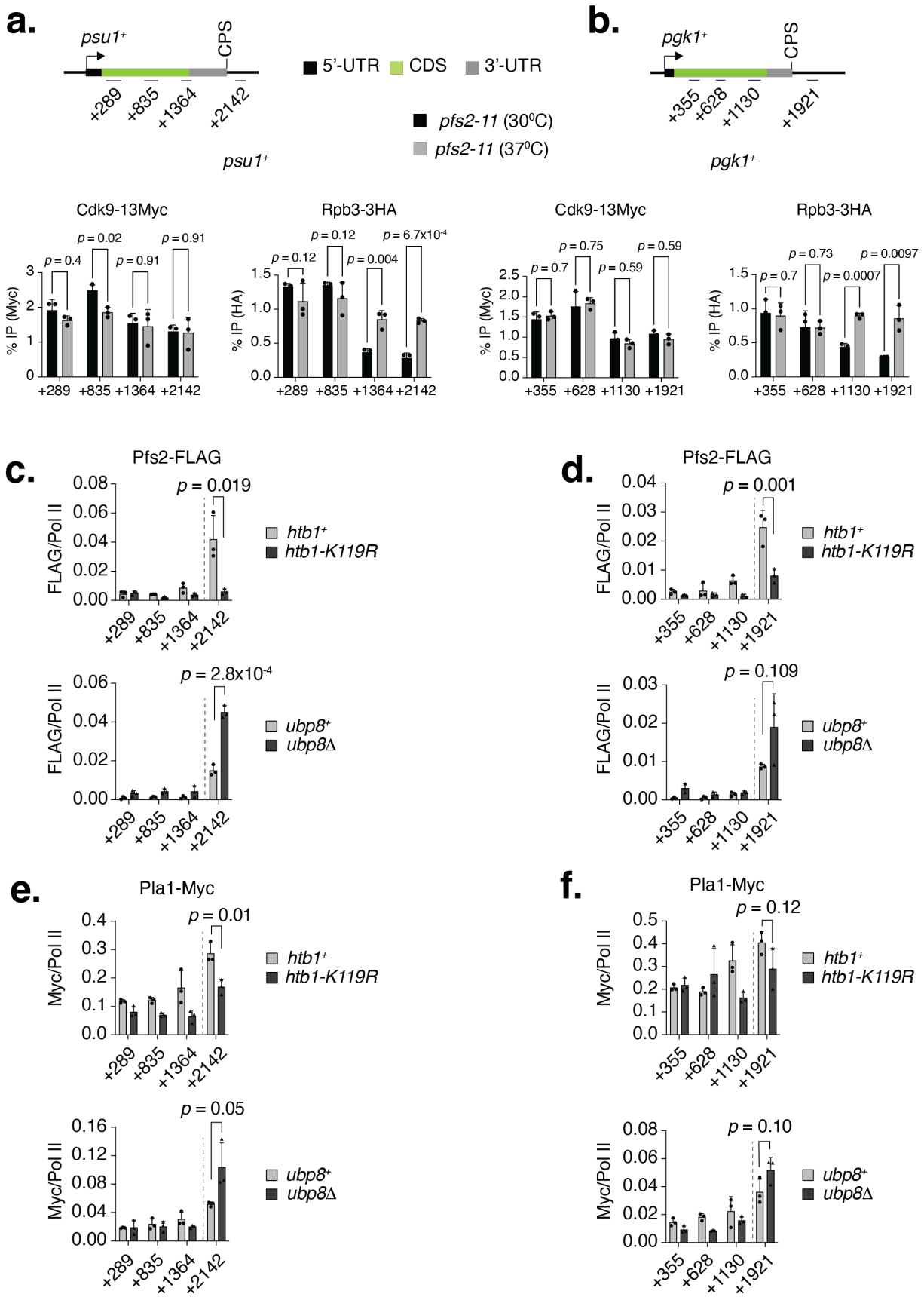
a.
psu1+
CPS
+289
+835
+1364
+2142
5'-UTR
CDS
3'-UTR
pfs2-11 (30⁰C)
pfs2-11 (37⁰C)
psu1+
b.
pgk1+
CPS
+355
+628
+1130
+1921
pgk1+
Cdk9-13Myc
% IP (Myc)
p = 0.4
p = 0.02
p = 0.91
p = 0.91
Rpb3-3HA
% IP (HA)
p = 0.12
p = 0.12
p = 0.004
p = 6.7x10-4
Cdk9-13Myc
% IP (Myc)
p = 0.7
p = 0.75
p = 0.59
p = 0.59
Rpb3-3HA
% IP (HA)
p = 0.7
p = 0.73
p = 0.0007
p = 0.0097
c.
Pfs2-FLAG
FLAG/Pol II
p = 0.019
htb1+
htb1-K119R
p = 2.8x10-4
ubp8+
ubp8Δ
d.
Pfs2-FLAG
FLAG/Pol II
p = 0.001
htb1+
htb1-K119R
p = 0.109
ubp8+
ubp8Δ
e.
Pla1-Myc
Myc/Pol II
p = 0.01
htb1+
htb1-K119R
p = 0.05
ubp8+
ubp8Δ
f.
Pla1-Myc
Myc/Pol II
p = 0.12
htb1+
htb1-K119R
p = 0.10
ubp8+
ubp8Δ

758

759 **Extended Data Figure 6 | Cdk9 evictions occur upstream of cleavage and**
760 **polyadenylation**. **a**, Chromatin distribution of Cdk9, where ChIP-qPCR results reveal no
761 alterations in Cdk9 occupancy on *psu1*$^+$ upon heat inactivation of Pfs2 at 37°C, while Pol II
762 occupancy on *psu1*$^+$ increased at the 3'-end of the gene under the same condition. **b**, ChIP-
763 qPCR analyses demonstrate no changes in Cdk9 occupancy on *pgk1*$^+$ upon heat inactivation of
764 Pfs2 at 37°C, with a concurrent increase in Pol II occupancy at the 3'-end of the gene of *pgk1*$^+$.
765 **c**, ChIP-qPCR results indicating a decrease in Pfs2 occupancy on *psu1*$^+$ in *htb1-K119R* cells
766 (top panel) and an increase in Pfs2 occupancy in *ubp8Δ* cells (bottom panel). **d**, ChIP-qPCR
767 results show a parallel pattern for *pgk1*$^+$, with decreased Pfs2 occupancy in *htb1-K119R* cells
768 (top panel) and increased occupancy in *ubp8Δ* cells (bottom panel). **e**, ChIP-qPCR results
769 demonstrating a decrease in Pla1 occupancy on *psu1*$^+$ in *htb1-K119R* cells (top panel) and an
770 increase in *ubp8Δ* cells (bottom panel). **f**, ChIP-qPCR reveals a decrease in Pla1 occupancy on
771 *pgk1*$^+$ in *htb1-K119R* cells (top panel) and an increase in *ubp8Δ* cells (bottom panel). For panels
772 **a**-**f**, individual data points were obtained from three independent biological replicates (n = 3).
773 One-sided error bars represent the standard deviation (s.d.) of mean ChIP values, and p-values
774 (Student's t-test) are indicated in the plots. Vertical dotted lines mark the CPS.
775

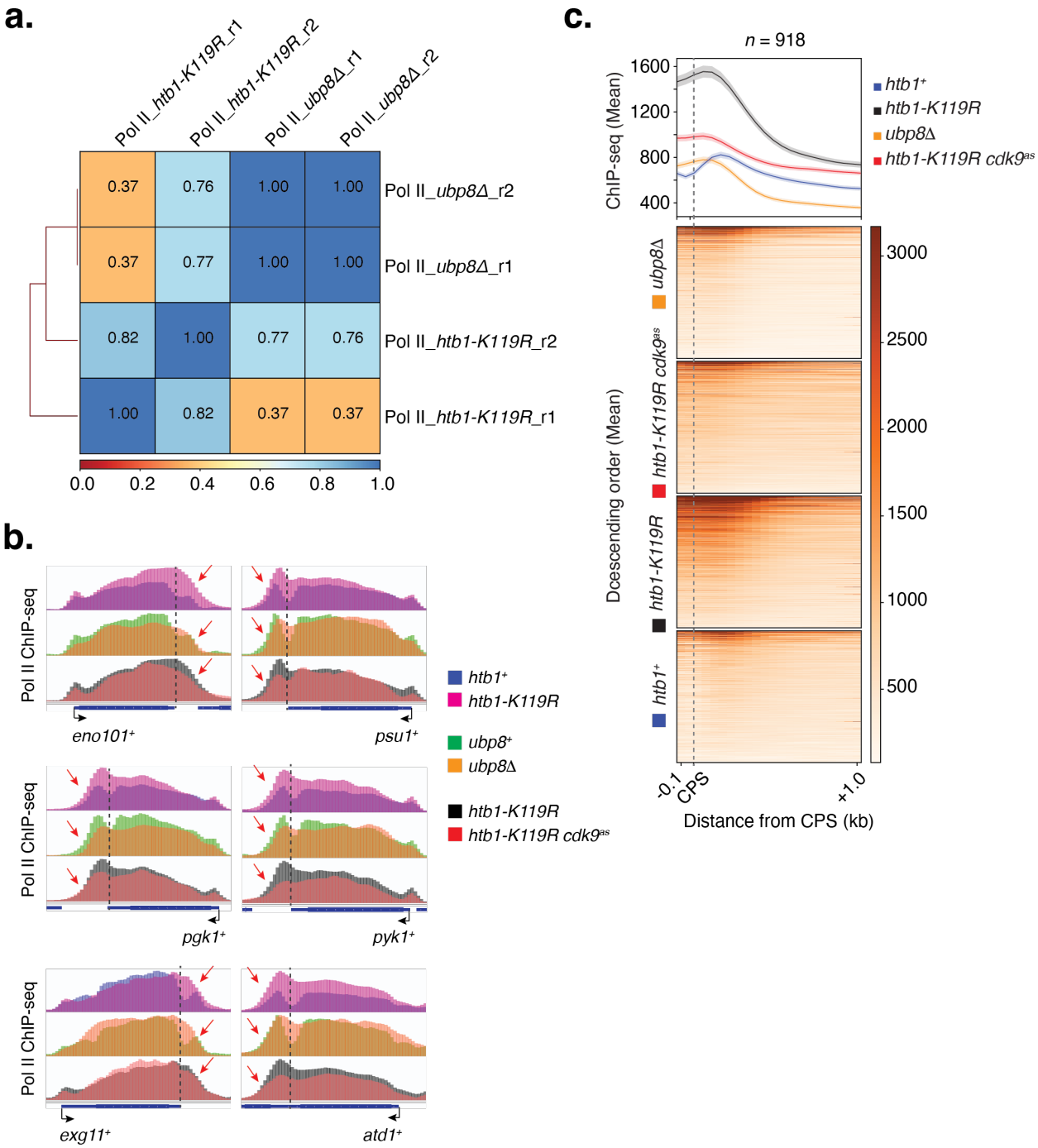

Extended Data Figure 7 | H2Bub1 regulates transcription termination. **a**, Correlation between Pol II ChIP-seq samples in *htb1-K119R* and *ubp8Δ* cells. Paired-end sequencing reads were mapped to the fission yeast genome using Bowtie2 (Galaxy Version 2.5.3+galaxy1). The correlation between pairs of replicates was calculated using mapped reads from each biological

781 replicate. Values in boxes represent the Pearson correlation coefficient between corresponding
782 samples (*n* = 2 biological replicates). **b**, Loss of H2Bub1 impairs termination. ChIP-seq browser
783 tracks reveal an extended Pol II distribution in *htb1-K119R* cells beyond the regular termination
784 zone seen in *htb1*$^{+}$ cells, indicating readthrough transcription, i.e., termination defects. The blue
785 and pink tracks, representing the Pol II distribution in *htb1*$^{+}$ and *htb1-K119R* cells, respectively,
786 are overlaid. Conversely, persistent levels of H2Bub1 favor termination. ChIP-seq browser
787 tracks show a narrowed Pol II distribution in the termination zone in *ubp8Δ* cells, indicating that
788 hyper mono-ubiquitylation favors termination. The green and orange tracks, representing the
789 Pol II distribution in *ubp8*$^{+}$ and *ubp8Δ* cells, respectively, are overlaid. Cdk9 inhibition in the
790 *htb1-K119R* background narrows Pol II distribution, suggesting a rescue of termination defects.
791 This indicates that the accumulation of Cdk9 following the loss of H2Bub1 is the main trigger for
792 termination defects by continuing elongation. The black and red tracks, representing the Pol II
793 distribution in *htb1-K119R*, with or without inhibition of Cdk9, respectively, are overlaid. Pol II
794 ChIP-seq data following Cdk9 inhibition in *htb1-K119R* cells, used in this analysis, were
795 obtained from a published study [16]. The regions of alterations in Pol II distribution after the CPS
796 are indicated by red arrows. **c**, Metagene analyses (top) and heatmaps (bottom) display a
797 genome-wide distribution of Pol II beyond the CPS of 1 kb separated genes (*n* = 918) in *htb1-*
798 *K119R* cells, both with and without Cdk9 inhibition, as well as in *ubp8Δ* cells. Metagene plots
799 further support global termination defects in *htb1-K119R* cells, proper termination upon hyper-
800 monoubiquitylation in *ubp8Δ* cells, and the rescue of termination defects in *htb1-K119R* cells
801 upon Cdk9 inhibition. The genes are sorted based on Pol II occupancy between regions -0.1 kb
802 to +1.0 kb of the CPS. For **b**,**c**, the vertical dotted lines mark the CPS. The Cdk9 inhibition ChIP-
803 seq data was used from previous report [16].
804

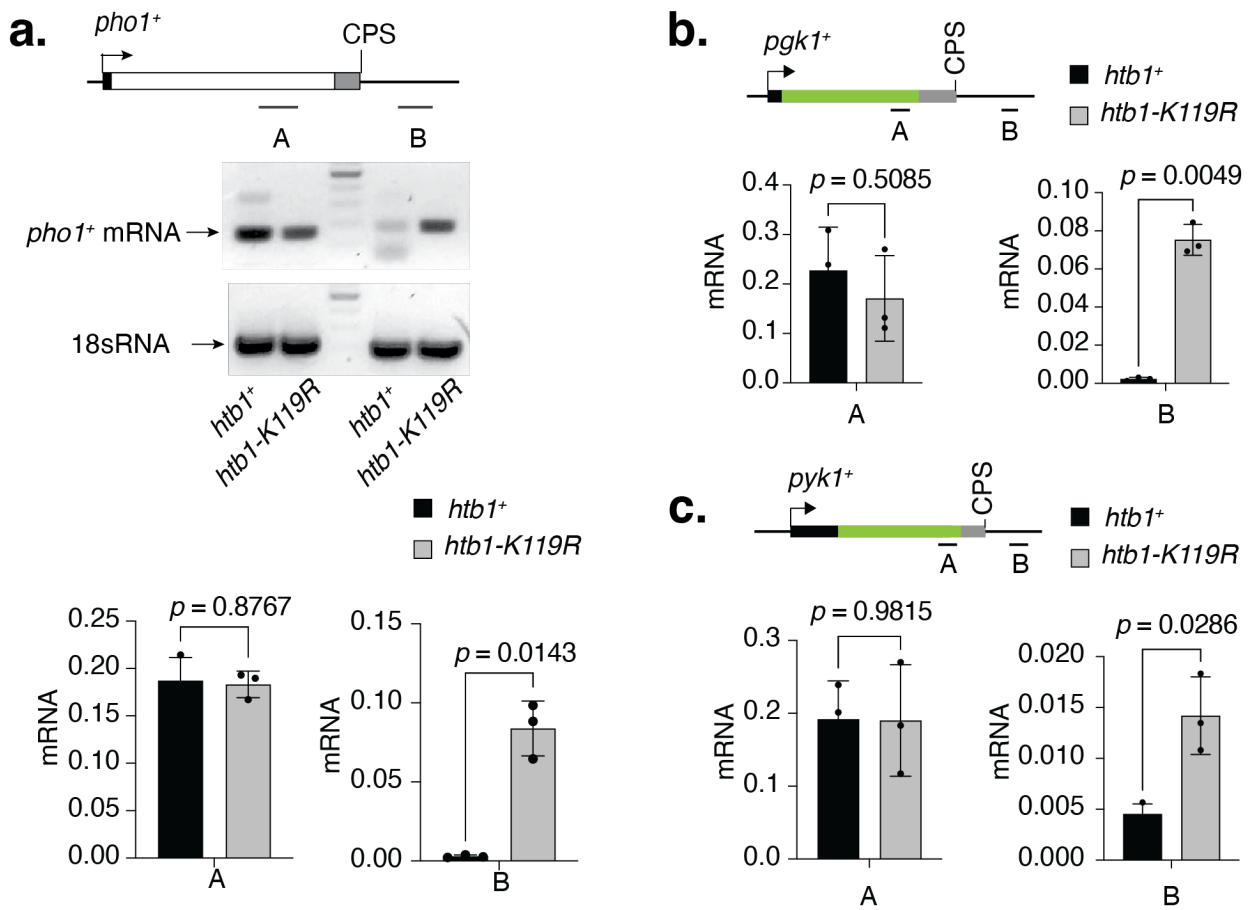

Extended Data Figure 8 | H2Bub1 regulates transcription termination. **a**, The top panel shows an agarose gel visualizing transcript production from the upstream (A) and downstream (B) regions of the CPS of the *pho1*$^{+}$ gene. The results indicate the synthesis of *pho1*$^{+}$ mRNA beyond the regular termination zone in *htb1-K119R* cells, with little to no mRNA synthesis in *htb1*$^{+}$ cells. The bottom panel shows RT-qPCR analyses quantifying *pho1*$^{+}$ mRNA production from the same regions, A and B, indicating increased mRNA synthesis beyond the termination zone in *htb1-K119R* cells. **b**, RT-qPCR analyses quantifying *pgk1*$^{+}$ mRNA production from the regions, A and B, indicating increased mRNA synthesis beyond the termination zone in *htb1-K119R* cells. **c**, RT-qPCR analyses quantifying *pyk1*$^{+}$ mRNA production from the regions, A and B, indicating increased mRNA synthesis beyond the termination zone in *htb1-K119R* cells. For panels **a**-**c**, individual data points shown in the plots were obtained from three independent

817 biological replicates (*n* = 3); two-sided error bars represent the standard deviation (s.d.) of mean

818 qRT-PCR values; *p*-values (Student's t-test) are indicated in the plots.

819

820

821

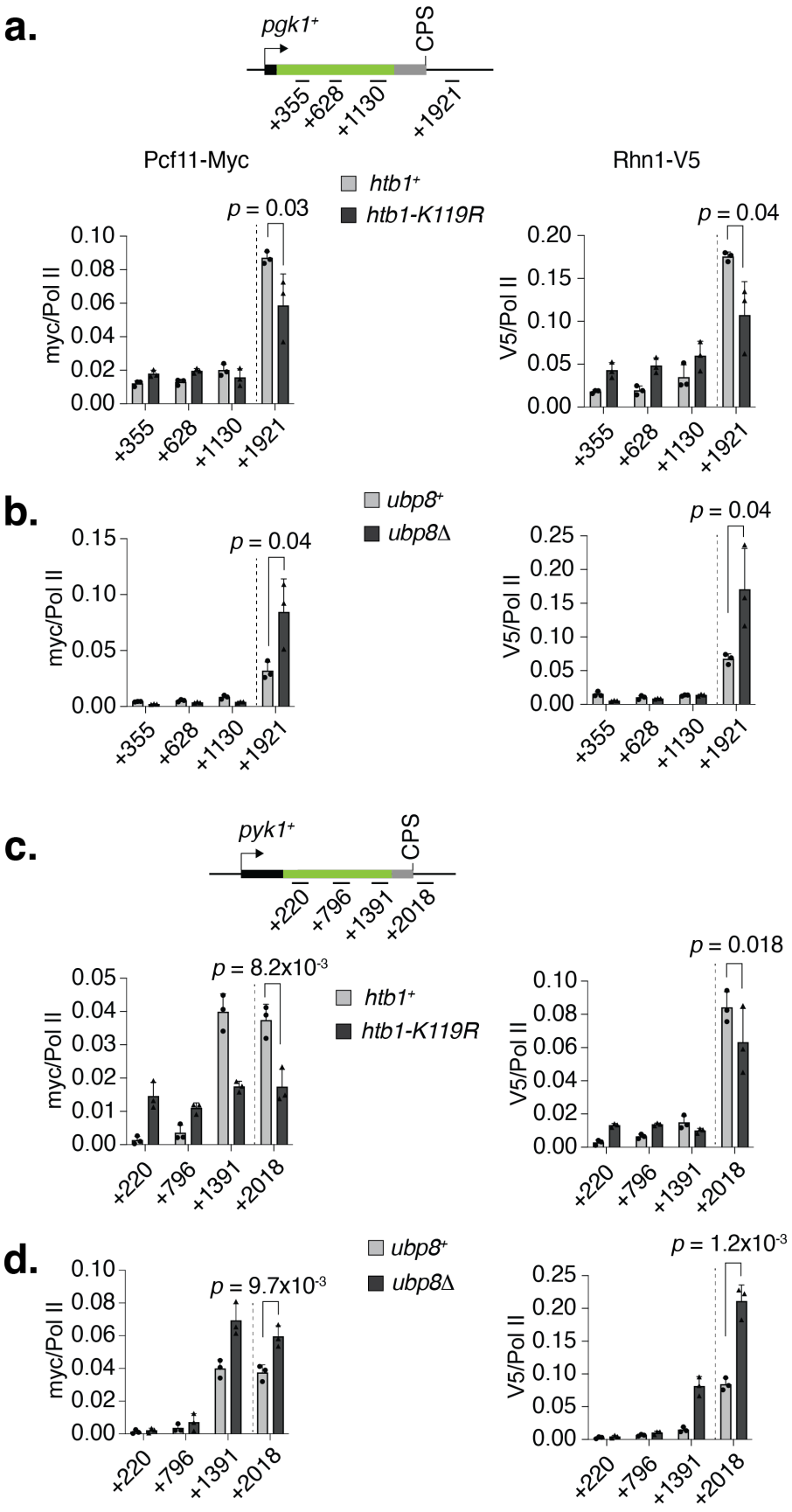
a.
pgk1+
CPS
+355
+628
+1130
+1921
Pcf11-Myc
Rhn1-V5
htb1+
htb1-K119R
p = 0.03
p = 0.04
myc/Pol II
V5/Pol II
b.
ubp8+
ubp8Δ
p = 0.04
p = 0.04
c.
pyk1+
CPS
+220
+796
+1391
+2018
p = 8.2x10-3
p = 0.018
d.
p = 9.7x10-3
p = 1.2x10-3

822

823 **Extended Data Figure 9 | H2Bub1 controls termination factor recruitment**. **a**, Distribution of
824 Pcf11 and Rhn1 on *pgk1*$^{+}$. ChIP-qPCR analyses show a significant decrease in the occupancy
825 of Pcf11 and Rhn1 in *htb1-K119R* cells. **b**, ChIP-qPCR analyses show a significant increase in
826 the occupancy of Pcf11 and Rhn1 in *ubp8Δ* cells. **c**, Distribution of Pcf11 and Rhn1 on *pyk1*$^{+}$.
827 ChIP-qPCR analyses show a significant decrease in the occupancy of Pcf11 and Rhn1 in *htb1-*
828 *K119R* cells. **d**, ChIP-qPCR analyses show a significant increase in the occupancy of Pcf11 and
829 Rhn1 in *ubp8Δ* cells. For panels **a**-**d**, experiments were performed with three independent
830 biological replicates (n = 3); one-sided error bars represent the standard deviation (s.d.) of
831 mean ChIP values. p-values (Student's t-test) are indicated in the plots. The CPS is marked by
832 dotted lines.
833

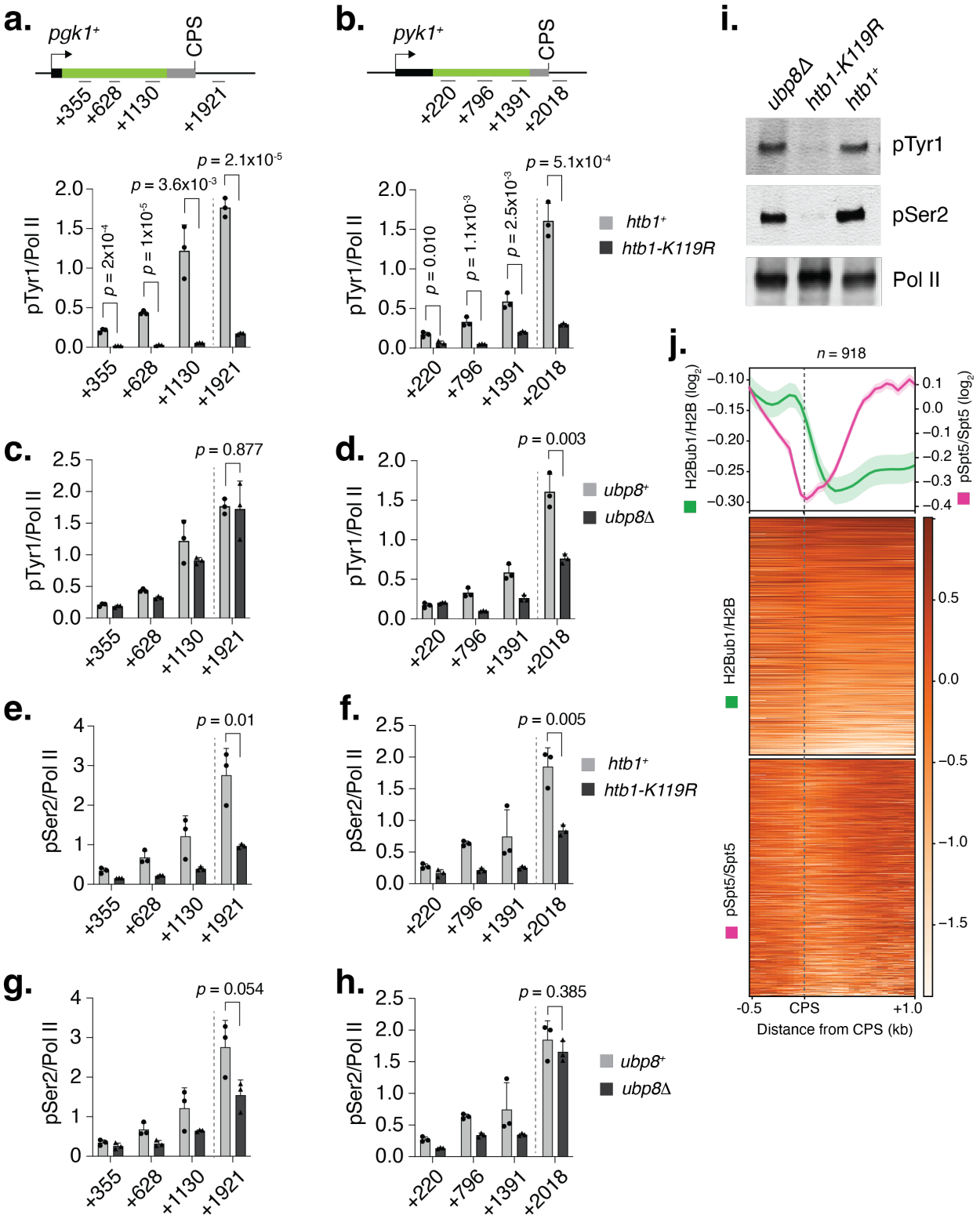

834

835 **Extended Data Figure 10 | H2Bub1 influences Pol II CTD Tyr1 and Ser2 phosphorylation**.

836 Distribution of Pol II CTD Tyr1 and Ser2 phosphorylation on *pgk1*$^+$ and *pyk1*$^+$. **a**, **b**, ChIP-qPCR

837 analyses indicate a significant reduction in Pol II CTD Tyr1 phosphorylation in *htb1-K119R* cells.
838 **c**, **d**, Panels reveal minimal to no change in Pol II CTD Tyr1 phosphorylation in *ubp8Δ* cells, as
839 demonstrated by ChIP-qPCR analyses. **e**, **f**, Similarly, illustrate a notable decrease in Pol II CTD
840 Ser2 phosphorylation in *htb1-K119R* cells through ChIP-qPCR analyses. **g**, **h**, Panels confirm
841 that *ubp8Δ* cells exhibit little to no change in Pol II CTD Ser2 phosphorylation according to
842 ChIP-qPCR analyses. All experiments (panels **a**-**h**) were conducted with three independent
843 biological replicates (n = 3); one-sided error bars represent the standard deviation (s.d.) of
844 mean ChIP values, and p-values (Student's t-test) are shown in the plots. The CPS is marked
845 by dotted lines. **i**, Immunoblot showing a loss of Pol II CTD Tyr1 (pTyr1) and Ser2 (pSer2)
846 phosphorylation in whole cell extracts of *htb1-K119R* cells, whereas these modifications remain
847 nearly unchanged in *ubp8Δ* cells. **j**, Metagene analyses (top) and heatmaps (bottom) display a
848 genome-wide distribution of pSpt5:Spt5 and H2Bub1:H2B around the CPS of 1 kb separated
849 genes (n = 918). The results indicate the accumulation of H2Bub1 upstream of the CPS, where
850 phospho-Spt5 gradually decays. The genes are sorted based on Pol II occupancy between
851 regions -0.5 kb to +1.0 kb of the CPS. H2B, H2Bub1, Spt5, pSpt5 ChIP-seq data used in this
852 analysis were obtained from a published study [16].
853
854
855
856
857
858
859
860
861
862

863

864 **Extended Data Table 1 | Yeast Strains**

Strain	Genotype	Source
JS78	*leu1-32 ura4-D18 his3-D1 ade6-M210 h*	[43]
LV239	*htb1-K119R-FLAG::kanMX6 spt5-13myc::kanMX6 leu1-32 ura4-D18 his3-D1 ade6-M21X h?*	[8]
LV259	*htb1-K119R-FLAG::kanMX6 cdk9-13myc::kanMX6 leu1-32 ura4-D18 his3-D1 ade6-M210 h?*	[8]
HD6-51	*cdk9-13myc::kanMX6 leu1-32 ura4-D18 his3-D1 ade6-M210 h+*	[44]
CS112	*cdk9T^{120G}::kanMX6 spt5-13myc::kanMX6 leu1-32 ura4-D18 his3-D1 ade6-*	[41]
CS172	*pch1-13myc::kanMX6 leu1-32 ura4-D18 his3-D1 ade6-M216 h*	[45]
VV1484	*dis2-3xFLAG::natMX6 h-*	[46]
TB4	*h+ cdk9-13myc::kanMX6 ubp8Δ::ura4*	This article
TB11	*rhn1-PK::hph pcf11-myc::kanMX6 htb1-K119R::kanMX6 h?*	This article
TB21	*dis2-3xFLAG::natMX6 htb1-K119R::kanMX6*	This article
TB27	*dis2-3xFLAG::natMX6 ubp8Δ::ura4*	This article
TB29	*rhn1-PK::hph pcf11-myc::kanMX6 ubp8Δ::ura4 h?*	This article
TB32	*pla1-myc::kanMX6 ubp8Δ::ura4*	This article
TB38	*pfs2-11 cdk9-myc::kanMX6 h+*	This article
TB54	*cdk9as::natMX6 htb1K119R::kanMX6 pfs2-FLAG::kanMX6*	This article

TB55	*pla1-myc::kanMX6 htb1K119R::kanMX6*	This article
TB57	*pfs2-FLAG::kanMX6 ubp8Δ::ura4*	This article
FY23510	*h90 leu1-32 ura4-D18 ade6-M210 red1-FLAG::kanMX6 pla1-myc::kanMX6*	Yeast Genetic Resource Center (YGRC), Japan
FY23525	*h90 leu1-32 ura4-D18 ade6-M210 or M216 rhn1-PK::hph pcf11-myc::kanMX6*	Yeast Genetic Resource Center (YGRC), Japan
FY23541	*h90 or h- leu1-32 ura4-D18 ade6-210 red5-myc::hph pfs2-FLAG::kanMX6*	Yeast Genetic Resource Center (YGRC), Japan

884

885

886 **Extended Data Table 2 | Oligonucleotides**

Name	Sequence	Direction	Amplicon
psu1-1F	GCCATCCTCATCACTTGCTT	Forward	+289
psu1-1R	GAGTAACTGAAGCGGCAACC	Reverse	
psu1-2F	TTGAGGGTGCCTACTGCTCT	Forward	+835
psu1-2R	TTGGCCAAGTGTGTTTTGAA	Reverse	
psu1-3F	TGATGGCGCTTCTGTTAGTG	Forward	+1364/A
psu1-3R	AATCCCCTACGTCCCAAATC	Reverse	
psu1-4F	GTTAGCAAAGCTGCGTTGTG	Forward	+2142
psu1-4R	GCAATGGTTAGTCCCTTTGG	Reverse	
psu1-6F	GAGCATGGTTTGATTGATATG	Forward	B
psu1-6R	CAGTTTAGAAATGTCTGAACC	Reverse	
pgk1-1F	CTTGAAGCCTGTTGCTGCTG	Forward	+355
pgk1-1R	GGATGACCTCACCACCCTTG	Reverse	
pgk1-2F	TCACCGTGCTCACTCCTCTA	Forward	+628
pgk1-2R	AAGATGGCAAGGAAGGGACG	Reverse	
pgk1-3F	GGTCCCGCTGGTGTCTTTG	Forward	+1130/A
pgk1-3R	AGACGTGGGAAAGAGCATCCT	Reverse	
pgk1-4F	CGCGTTGCTCTATCCATCGG	Forward	+1921
pgk1-4R	TCGCAAGCAAAAAATCCACGG	Reverse	
pgk1_6F	CACTAGATTCAAGCTTGAACCTG	Forward	B
pgk1_6R	CGCTTAGATGAACTGTGCCG	Reverse	
pyk1-1F	CAACGTTGAGACCTTGTGCA	Forward	+220
pyk1-1R	TCGTCGGTGGTGAAGATCAT	Reverse	
pyk1-2f	CCGTGAAGTTTTGGGTGAGG	Forward	+796
pyk1-2R	TTGGGCGACGAAAACTTGAG	Reverse	
pyk1-3F	ATGGTTACTCGTTGCCCTCA	Forward	+1391/A
pyk1-3R	AGACGGAAGATGGAGGTGTG	Reverse	
pyk1-4F	GCGAAAAGTGCCTGATGAA	Forward	+2018
pyk1-4R	ATTCCCATTGCTCTGGCTTA	Reverse	
pyk1_9F	AGCTAAGCCAGAGCAATGGG	Forward	B
pyk1_9R	CTCTTCAGAATCTACGTTCC	Reverse	
pho1_GeneBody_F2	TCTTTGGAGGTGCCTATGCT	Forward	A
pho1_GeneBody_R2	CCAGCAAATGGGACAAATTC	Reverse	
pho1_RT_F4	CAGTTAAGACACTTTCAGCCC	Forward	B
pho1_RT_R4	GTTTCATCGTAGCACTTCATACG	Reverse	
cMYC			
PP562	GTAGTTAATTCATGCGGCTCTCTTACT	Forward	-200
PP563	GGGCAGCCGAGCACTCTA	Reverse	
PP564	GGAGGGATCGCGCTGAGTA	Forward	+1

PP565	TCTGCCTCTCGCTGGAATTAC	Reverse	
PP566	GCCGCATCCACGAAACTTT	Forward	+190
PP567	TCCTTGCTCGGGTGTTGTAAG	Reverse	
PP568	TGCCCCTCAACGTTAGCTTC	Forward	+2018
PP569	GGCTGCACCGAGTCGTAGTC	Reverse	
PP570	GTCCAAAGCCTCATTAAGTCTTAGGTA	Forward	+3589
PP571	CAACTTCCCAGGATAGGACATTG	Reverse	
PP572	AAGTACATTTTGCTTTTTAAAGTTGATT	Forward	+5155
PP573	GGCTCAATGATATATTTGCCAGTTATTTTA	Reverse	
PP574	TCCCCATATTAGAAGTAGAGAGGGAA	Forward	+6028
PP575	CTTGGGCATGTGGATGAGTCT	Reverse	
PP576	TGAAGGATGTTGGAGCATGAGTA	Forward	+11382
PP577	TCTCTTCCCAGTTGAGTCTTGAAA	Reverse	
GAPDH			
PP655	CAATTCCCCATCTCAGTCGT	Forward	-300
PP656	GCAGCAGGACACTAGGGAGT	Reverse	
PP657	CTCCTGTTCGACAGTCAGC	Forward	+55
PP658	TTCAGGCCGTCCCTAGC	Reverse	
PP659	AAGTCAGGTGGAGCGAG	Forward	+929
PP660	TAAACCCACTTCTTTGATTTACCAGAG	Reverse	
PP663	CACCCTGGTCTGAGGTTAAATATAG	Forward	+1407
PP664	GTGGGAGCACAGGTAAGT	Reverse	
PP665	CCCTGTGCTCAACCAGT	Forward	+3882
PP666	CTCACCTTGACACAAGCC	Reverse	
PP667	AGATGTGTCAGGGTGACTTAT	Forward	+4511
PP668	TAGGTCCCAGCTACACGC	Reverse	
PP669	CCTATACCGAGGCATTGTGAA	Forward	+5100
PP670	GCTTCCTCCGTGTCTGTCATA	Reverse	
PP671	TTCACATTCCTGATACGTGGACAA	Forward	+5747
PP672	CGTGGGTGTCTGCTACT	Reverse	
VEGFA			
-941_hVEGFA_F	TCACTGACTAACCCCGGAAC	Forward	-941
-941_hVEGFA_R	GCCTGCAGACATCAAAGTGA	Reverse	
+148_hVEGFA_F	TCCGGGTTTTATCCCTCTTC	Forward	+148
+148_hVEGFA_R	TCTGCTGGTTTCCAAAATCC	Reverse	
+1947_hVEGFA_F	AGACCCTACCTCTGCCCAGT	Forward	+1947
+1947_hVEGFA_R	GCCACGACTTCTGACAGTGA	Reverse	
+2958_hVEGFA_F	TGTGACCTTGGCTGTCTCTG	Forward	+2958
+2958_hVEGFA_R	CTCCAGCTCTCACCAACTCC	Reverse	
+4158_hVEGFA_F	AAGGAGGAGGGCAGAATCAT	Forward	+4158
+4158_hVEGFA_R	GACCTGAACAGCGGAGAGTC	Reverse	
+7428_hVEGFA_F	CCCACTGAGGAGTCCAACAT	Forward	+7428
+7428_hVEGFA_R	CATACCTCCCCTGTGCAACT	Reverse	
+12840_hVEGFA_F	TACTGGGGACCAAGGAAGTG	Forward	+12840

+12840_hVEGFA_R	AGTCTTGCCTCCCTGACTGA	Reverse	
+18362_hVEGFA_F	CACTGGCTGTCCTCTCTTCC	Forward	+18362
+18362_hVEGFA_R	AGGGATGGTGAAAAGGAGGT	Reverse	
ERRFI1			
-1168_hERRFI1_F	CTCTCCAAAGCCAAAAGACG	Forward	-1168
-1168_hERRFI1_R	TGACTGCGTTGGAATATGGA	Reverse	
-121_hERRFI1_F	GGCATCGCCCCTTTAAGC	Forward	-121
-121_hERRFI1_R	GCTCCCGCTAGCACTCTG	Reverse	
+681_hERRFI1_F	CACCGTGTACCCGTAAATCC	Forward	+681
+681_hERRFI1_R	TTTTGCAGTCCGATTCCATT	Reverse	
+2228_hERRFI1_F	AGGAGCAGAGGAAGGAAAGG	Forward	+2228
+2228_hERRFI1_R	CCGCAAAGGATGCTAAATGT	Reverse	
+3553_hERRFI1_F	GTTTCTGTTCCTGCCTCTGC	Forward	+3553
+3553_hERRFI1_R	CAGCATTTTCCCCACACTTT	Reverse	
+6777_hERRFI1_F	CAGGGGGAAAGCATAAATCA	Forward	+6777
+6777_hERRFI1_R	AGCTCTACCCTGCCTTCTCC	Reverse	
+9857_hERRFI1_F	GGGTGTTTCACAAAGGAGGA	Forward	+9857
+9857_hERRFI1_R	TGGGGAGACAAATTCTCCAG	Reverse	
+11709_hERRFI1_F	CTTTGAACCACACCATGTGC	Forward	+11709
+11709_hERRFI1_R	ATTCATCGGAGCAGATTTGG	Reverse	